A multiscale model for nickel-based directionally solidified materials

F. Coudon, G. Cailletaud, J. Cormier, L. Marcin

Version of Record: https://www.sciencedirect.com/science/article/pii/S0749641918302341
Manuscript_8c0345f09fa59cae8d736c2a8a904b73

A multiscale model for Nickel-based directionally solidified materials

F. Coudon[a,b], G. Cailletaud[a], J. Cormier[c], L. Marcin[b]

[a] *MINES ParisTech, PSL Research University, MAT - Centre des Matériaux, CNRS UMR 7633, BP 87 91003 Evry, FRANCE*
[b] *Safran Tech, Safran Group, rue des jeunes bois, 78172, Chateaufort, FRANCE*
[c] *Institut Pprime, UPR CNRS 3346, ISAE-ENSMA, 1 avenue Clément Ader, BP40109 86961 Futuroscope Chasseneuil, FRANCE*

Abstract

In this paper, the so-called "β rule" is used to simulate the anisotropic behaviour of directionally solidified superalloys. First, the "mean-field" model is extended to the general case of heterogeneous local elasticity. Two other models also designed using the "self-consistent" framework are applied to make comparisons, either with the assumption of a purely elastic accommodation of grains (Kröner-Weng model) or the translated field theory. As a reference, full-field simulations using a representative volume element (RVE) and a crystal plasticity finite element model (CPFEM) are carried out. Results show that the β rule is able to predict the overall response of the material for various cases such as one-dimensional or two-dimensional cyclic loading with or without a mean stress. Otherwise, local estimations are studied for both mean-field and full-field models. The local responses of the β rule are consistent when they are compared to those of CPFE simulations.

Keywords: Anisotropic material, constitutive behaviour, crystal plasticity, polycrystalline material

1. Introduction

Directionally solidified (DS) nickel base superalloys receive a renewed interest for the design of turbine blades [1, 2, 3]. Indeed, the temperatures within the gas chamber still increase in order to create more efficient gas turbines and thereby lead to severe thermomechanical conditions for downstream components. The interest of DS alloys comes from the columnar

Email addresses: florent.coudon@safrangroup.com (F. Coudon), georges.cailletaud@mines-paristech.fr (G. Cailletaud), jonathan.cormier@ensma.fr (J. Cormier), lionel.marcin@safrangroup.com (L. Marcin)

shape of grains along a macroscopic axis (chosen as X_3 in the sequel). This axis is commonly chosen as colinear to the main centrifugal loading applied to turbine blades. By eliminating perpendicular grain boundaries, the fatigue and creep resistance of DS alloys are significantly improved against untextured materials [4]. Moreover, keeping a thermal gradient in control during casting allows to conserve a viscous molten metal, so that more and more thin turbine blades can be produced. For these reasons, DS materials still remain good candidates for low pressure turbine blades of modern aero-engines. In addition, the axis of cylindrical grains is colinear to a $\langle 001 \rangle$ crystallographic direction of the face centered cubic (FCC) lattice structure (see the Fig. 1), generating a strong elastic and plastic anisotropy.

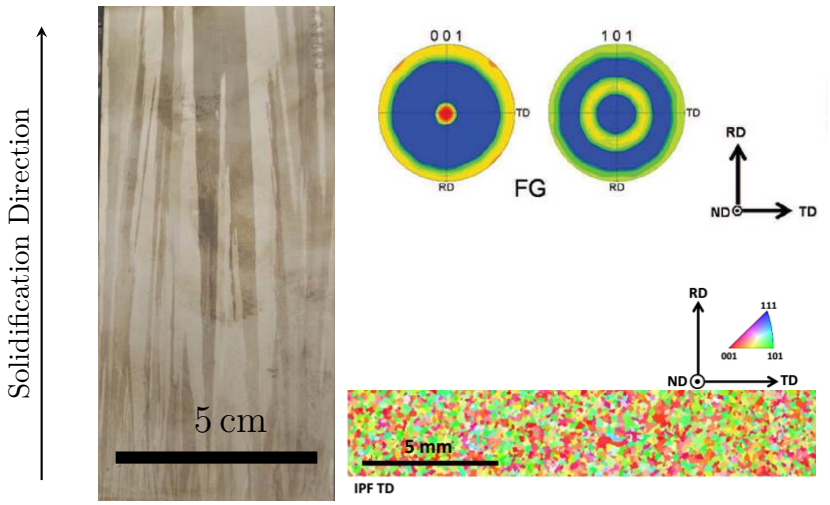

Figure 1: Plate made in DS200+Hf and Electron backscatter diffraction (EBSD) analysis in a cross section showing the material texture [5].

Accordingly, the mechanical behaviour of these alloys takes place at the border line between a single crystal and a polycrystalline aggregate. "Level 1" purely macroscopical models are widely used to predict the behaviour of DS alloys [6, 7, 8], considering a transverse isotropic symmetry. Generally, the calibration is made using one-dimensional experimental tests. Doing so, the predictive response of the model may not be reliable for multi-axial loadings as it is imposed to 3D components. In this paper, another strategy for DS alloys based on "mean field" modeling [9, 10] is discussed, which introduces rigorously both the anisotropy due to the behaviour of grains seen as single crystals and the anisotropy induced by the morphology

and the crystallographic texture of this kind of material.

The pioneering work of Taylor [11] in the homogenization of metals demonstrates the interest of introducing local behaviour of grains to predict plastic flow of polycrystalline aggregates. Classically, a scale transition rule allows to pass from the global strain or stress to local quantities within each phase[1]. This is the "localization" step. The corresponding analytical expression can be highly nonlinear in time or/and in space if complex interactions between grains are considered (viscous interactions, memory effect, ...) or if field fluctuations within each phases are searched. After this stage, each phase is independently applied a single crystal model. The second step called "homogenization" defines global quantities related to ones computed for each phase, like the overall plastic strain, ... Considering the size, shape and orientation of grains, the definition of a homogeneous equivalent medium (HEM) searched as a weighted average of each phase contribution is assumed, well known as the self-consistent approach [12, 13]. Frequently, these "Level 2" methods are seen as computational intensive approach, so that "Level 1" models were promoted [6] for industrial applications, specifically with the number of phases which have to be considered for metals. Such a situation can be relieved by using optimal localization rules where non linear phenomena are simplified and the numerical convergence of the model integration is fast. In this way, a pragmatic solution consists in describing the non linear plastic accommodation of the phases by means of a second level of hardening at the aggregate scale, using a phenomenological form, as proposed by the "β models" [14, 15]. This method gives the opportunity to formulate an explicit estimate of the local stress as a function of the macroscopic stress and strain, and of the local strain. The model was previously used to simulate cyclic responses of untextured polycrystalline aggregates [16]. The transition rule, first developed with the assumption of isotropic inclusions, was extended to anisotropic materials in Saï *et al* [10]. As seen recently in Martin *et al* [17], the β model was not able to represent the elastic/plastic transition, compared to other models.

This paper presents a new extension of the "β model" also adapted to directionally solidified aggregates but introducing both elastic and plastic heterogeneous responses of grains. Section 2 shows the equations of the new micro-mechanical model using the self-consistent scheme. In section 3, a numerical identification of the intergranular hardening is presented. Other

[1]In the sequel, the use of the term "phase" refers to a domain with specific local mecanical properties in a heterogeneous material as a particle, a fiber or grains with a given crystallographic orientation

homogenization techniques are introduced to evaluate the capabilities of the proposed model, a simpler model which assumes purely elastic interaction between grains and another which introduces more complex schemes as the so-called translated fields to significantly account for viscous effects. Two elementary cases of pure tensile and pure shear loading are used to calibrate the β model. In this work, we have paid attention to the local responses provided by micro-mechanical models by comparing them with "reference" curves obtained by means of several full-field simulations. Section 4 presents additional comparisons for more complex numerical tests like one-dimensional and multiaxial cyclic loadings. Some parameters which control the hardening at the grain scale are modified in order to demonstrate the capabilities of the model to represent cyclic hardening or ratchetting.

2. A micro-mechanical model adapted to directionally solidified alloys

First, the local behaviour of grains is fixed, considering the crystal plasticity model proposed by Meric *et al* [18] for Ni-based single crystal superalloys. The model uses the classical framework of crystal plasticity in small strain. Twelve FCC slip systems are considered. The equations (2) below recall how the plastic strain rate for the grain g, $\underset{\sim}{\dot{\varepsilon}}^{gp}$, is deduced from the value of the stress tensor for this grain, $\underset{\sim}{\boldsymbol{\sigma}}^{\mathrm{g}}$.

$$\begin{aligned}
\tau^s &= \underset{\sim}{\boldsymbol{m}}^s : \underset{\sim}{\boldsymbol{\sigma}}^{\mathrm{g}} = \frac{1}{2}\left(\vec{n}^s \otimes \vec{l}^s + \vec{l}^s \otimes \vec{n}^s\right) : \underset{\sim}{\boldsymbol{\sigma}}^{\mathrm{g}} \\
\dot{\gamma}^s &= \left\langle \frac{|\tau^s - x^s| - r^s}{K} \right\rangle^n \eta^s \\
x^s &= c\alpha^s \ , \ \dot{\alpha}^s = \dot{\gamma}^s - d\dot{v}^s\alpha^s \text{ and } \dot{v}^s = \eta^s\dot{\gamma}^s \\
r^s &= \tau^c + \sum_{r\neq s} Q\underset{\sim}{\boldsymbol{H}}^{rs}(1 - e^{-bv^r}) \\
\underset{\sim}{\dot{\varepsilon}}^{gp} &= \sum_s \dot{\gamma}^s \underset{\sim}{\boldsymbol{m}}^s
\end{aligned} \tag{1}$$

where $\underset{\sim}{\boldsymbol{m}}^s$ represents the orientation tensor of the s system defined by the symmetric part of the tensor product of the normal $\vec{n}^s$ and a slip direction $\vec{l}^s$ of one octahedral slip plane. τ^s is the resolved shear stress, $\dot{\gamma}^s$ is the shear rate and $\eta^s = sign(\tau^s - x^s)$. The Macauley brackets are defined as $\langle p \rangle = max(p, 0)$. The material parameters for the plastic flow are τ_c for the critical resolved shear stress, c and d for the kinematic hardening and Q and b for the isotropic hardening. The slip interaction matrix, H^{rs}, is chosen as the identity matrix.

The local behaviour of a grain being defined, a scale transition rule has to be applied

to access the mechanical properties of polycrystalline aggregates. A first solution is to find it numerically by using a full field approach. Then, simulations are carried out on a representative volume element of the material (realistic using Xray tomography [19] or synthetic by a Voronoï tessellation) and are solved by either a crystal plasticity finite elements method (CPFEM) [20, 21, 22] or a fast Fourier transform algorithm (CPFFT) [23, 24]. In another hand, this paper is focused on mean field approaches, where the scale transition rule is approximated analytically. In such a case, various strategies had been proposed in the literature as the self-consistent scheme [12, 13], the variational method [25, 26], the transformation field analysis (TFA) [27] [28], ... For the self-consistent scheme, the heterogeneous material is reduced to a collection of simple problems, represented by an inclusion embedded in a searched homogeneous equivalent media (HEM). Each inclusion (also called a crystallographic phase in the sequel) is defined by a crystal orientation and a simplified shape (a cylinder for DS alloys). Then the common track consists in solving analytically the inclusion problems by using either the exact Eshelby's solution [29] if the local phases are linear elastic or extended solutions for more complex behaviour [30]. In this work, a particular point is the use of a "phenomenological" transition rule, introducing parameters which have to be identified. In these works, these parameters are adjusted to provide similar results compared to CPFE simulations.

2.1. Some previous works

This section addresses only to first order mean field models which consist in estimating "per phase" average values of the stress and strain tensors. This assumption comes from the Eshelby's solution for a cylindrical inclusion whereas in full field approaches, polyhedral grains involve field fluctuations. More sophisticated models take into account this heterogeneity but are not within the main scope of this paper [31, 32]. The local quantities such as strain or stress tensors are identified by superscript g and refer to a cylindrical crystallographic phase with a crystal orientation ϕ_1 around the longitudinal axis (the other Euler's angles Φ and ϕ_2 are supposed to be equal to zero for perfect DS alloys) and volume fraction f^g (see the "Local scale" rectangle of Fig. 2). For a purely linear elastic behaviour, the local stress and strain in a grain are expressed by:

$$\underset{\sim}{\boldsymbol{\sigma}}^{\mathrm{g}} = \underset{\approx}{\boldsymbol{C}}^{g} : \underset{\sim}{\boldsymbol{\varepsilon}}^{\mathrm{g}} \qquad ; \qquad \underset{\sim}{\boldsymbol{\varepsilon}}^{\mathrm{g}} = \underset{\approx}{\boldsymbol{S}}^{g} : \underset{\sim}{\boldsymbol{\sigma}}^{\mathrm{g}} \tag{2}$$

For DS nickel-based superalloys, the local elasticity tensor, $\underset{\approx}{\boldsymbol{C}}^g$ and the local compliance $\underset{\approx}{\boldsymbol{S}}^g$ have a cubic symmetry. Otherwise, the overall stress is defined by a volume average of the local stress. The same applies to compute the macroscopic strain, so that an equation similar to Eq. 2 is written at the global scale, defining an effective elasticity tensor $\underset{\approx}{\boldsymbol{C}}$ and a global compliance $\underset{\approx}{\boldsymbol{S}}^{el}$:

$$\underset{\sim}{\boldsymbol{\Sigma}} = \underset{\approx}{\boldsymbol{C}} : \underset{\sim}{\boldsymbol{E}} \qquad ; \qquad \underset{\sim}{\boldsymbol{E}} = \underset{\approx}{\boldsymbol{S}}^{el} : \underset{\sim}{\boldsymbol{\Sigma}} \tag{3}$$

The Eshelby solution [29] provides a concentration law which links the local stress to the macroscopic stress, and a residual stress induced by the local and global strains:

$$\underset{\sim}{\boldsymbol{\sigma}}^{\mathrm{g}} = \underset{\sim}{\boldsymbol{\Sigma}} + \underset{\approx}{\boldsymbol{C}} : \left(\underset{\approx}{\boldsymbol{S}}_C^{-1} - \underset{\approx}{\boldsymbol{I}} \right) : (\underset{\sim}{\boldsymbol{E}} - \underset{\sim}{\boldsymbol{\varepsilon}}^{\mathrm{g}}) \tag{4}$$

where $\underset{\approx}{\boldsymbol{I}}$ is the fourth order identity tensor and $\underset{\approx}{\boldsymbol{S}}_C$ is the Eshelby tensor computed with respect to the effective elasticity tensor. Two localization tensors, $\underset{\approx}{\boldsymbol{B}}^g$ and $\underset{\approx}{\boldsymbol{A}}^g$, are then introduced to respectively link the local stress to the global stress and the local strain to the global strain:

$$\left\{ \begin{array}{rcl} \underset{\sim}{\boldsymbol{\sigma}}^{\mathrm{g}} & = & \underset{\approx}{\boldsymbol{B}}^g : \underset{\sim}{\boldsymbol{\Sigma}} \\ \underset{\sim}{\boldsymbol{\varepsilon}}^{\mathrm{g}} & = & \underset{\approx}{\boldsymbol{A}}^g : \underset{\sim}{\boldsymbol{E}} \\ \underset{\approx}{\boldsymbol{B}}^g & = & \left[\underset{\approx}{\boldsymbol{C}} : \underset{\approx}{\boldsymbol{C}}^{g-1} + \underset{\approx}{\boldsymbol{C}} : \underset{\approx}{\boldsymbol{S}}_C : \left(\underset{\approx}{\boldsymbol{C}}^{-1} - \underset{\approx}{\boldsymbol{C}}^{g-1} \right) \right]^{-1} \\ \underset{\approx}{\boldsymbol{A}}^g & = & \left[\underset{\approx}{\boldsymbol{I}} - \underset{\approx}{\boldsymbol{S}}_C : \left(\underset{\approx}{\boldsymbol{I}} - \underset{\approx}{\boldsymbol{C}}^{-1} : \underset{\approx}{\boldsymbol{C}}^g \right) \right]^{-1} \end{array} \right. \tag{5}$$

The local and global tensors are linked by the following relations:

$$\left\{ \begin{array}{rcl} \underset{\approx}{\boldsymbol{C}}^{-1} & = & \underset{\approx}{\boldsymbol{S}}^{el} = \left\langle \underset{\approx}{\boldsymbol{S}}^g : \underset{\approx}{\boldsymbol{B}}^g \right\rangle \\ \underset{\approx}{\boldsymbol{C}} & = & \left\langle \underset{\approx}{\boldsymbol{C}}^g : \underset{\approx}{\boldsymbol{A}}^g \right\rangle \end{array} \right. \tag{6}$$

For the case of an elasto-viscoplastic behaviour at the local scale, the expression of a concentration law is not a trivial task. Both the non linear form of local equations and the time dependency of the stress state at different orders need additional hypotheses. In the theoretical case of time-independent plasticity, Hill proposed the use of a linear tangent tensor [30] $\underset{\approx}{\boldsymbol{L}}^g$, defined in a rate form:

$$\dot{\underset{\sim}{\boldsymbol{\sigma}}}^{\mathrm{g}} = \underset{\approx}{\boldsymbol{L}}^g : \dot{\underset{\sim}{\boldsymbol{\varepsilon}}}^{\mathrm{g}} \tag{7}$$

An Eshelby-type problem is solved at each time increment, defining a "stress-free" strain rate proportionally to the local strain rate within the inclusion. The transition rule is expressed

incrementally using the assumption of a homogeneous stress rate field within the inclusion:

$$\dot{\underset{\sim}{\boldsymbol{\sigma}}}^{\mathrm{g}} = \dot{\underset{\sim}{\boldsymbol{\Sigma}}} + \underset{\approx}{\boldsymbol{L}} : \left(\underset{\approx}{\boldsymbol{S}}_{L}^{-1} - \underset{\approx}{\boldsymbol{I}} \right) : (\dot{\underset{\sim}{\boldsymbol{E}}} - \dot{\underset{\sim}{\boldsymbol{\varepsilon}}}^{\mathrm{g}}) \tag{8}$$

The fourth order tensor $\underset{\approx}{\boldsymbol{L}}$ represents the effective elastoplastic tangent tensor and the Eshelby tensor, $\underset{\approx}{\boldsymbol{S}}_{L}$, is then computed with respect to this tangent tensor. For an anisotropic elastic behaviour at the grain scale, Eq. 8 can be developed, using a decomposition of the strains as the sum of thermal, elastic and viscoplastic contributions, according to:

$$\underset{\approx}{\boldsymbol{S}}_{L} : \underset{\approx}{\boldsymbol{L}}^{-1} : \dot{\underset{\sim}{\boldsymbol{\sigma}}}^{\mathrm{g}} = \underset{\approx}{\boldsymbol{S}}_{L} : \underset{\approx}{\boldsymbol{L}}^{-1} : \dot{\underset{\sim}{\boldsymbol{\Sigma}}} + \left(\underset{\approx}{\boldsymbol{I}} - \underset{\approx}{\boldsymbol{S}}_{L} \right) : \left[\underset{\approx}{\boldsymbol{C}}^{-1} : \dot{\underset{\sim}{\boldsymbol{\Sigma}}} + \dot{\underset{\sim}{\boldsymbol{E}}}^{\mathrm{p}} + \underset{\sim}{\boldsymbol{\alpha}} \dot{T} - \underset{\approx}{\boldsymbol{C}}^{g\,-1} : \dot{\underset{\sim}{\boldsymbol{\sigma}}}^{\mathrm{g}} - \dot{\underset{\sim}{\boldsymbol{\varepsilon}}}^{gp} - \underset{\sim}{\boldsymbol{\alpha}}^{g} \dot{T} \right]$$

$$\begin{cases} \underset{\approx}{\boldsymbol{B}}_{L}^{g\,-1} : \dot{\underset{\sim}{\boldsymbol{\sigma}}}^{\mathrm{g}} &= \underset{\approx}{\boldsymbol{B}}_{L} : \dot{\underset{\sim}{\boldsymbol{\Sigma}}} + \underset{\approx}{\boldsymbol{C}}^{*} : (\dot{\underset{\sim}{\boldsymbol{E}}}^{\mathrm{p}} - \dot{\underset{\sim}{\boldsymbol{\varepsilon}}}^{gp}) + \underset{\approx}{\boldsymbol{C}}^{*} : (\underset{\sim}{\boldsymbol{\alpha}} - \underset{\sim}{\boldsymbol{\alpha}}^{g})\, \dot{T} \\ \underset{\approx}{\boldsymbol{B}}_{L}^{g} &= \left[\underset{\approx}{\boldsymbol{C}} : \underset{\approx}{\boldsymbol{S}}_{L} : \underset{\approx}{\boldsymbol{L}}^{-1} + \underset{\approx}{\boldsymbol{C}}^{*} : \underset{\approx}{\boldsymbol{C}}^{g\,-1} \right]^{-1} \\ \underset{\approx}{\boldsymbol{B}}_{L} &= \left[\underset{\approx}{\boldsymbol{C}} : \underset{\approx}{\boldsymbol{S}}_{L} : \underset{\approx}{\boldsymbol{L}}^{-1} + \underset{\approx}{\boldsymbol{C}}^{*} : \underset{\approx}{\boldsymbol{C}}^{-1} \right] \\ \underset{\approx}{\boldsymbol{C}}^{*} &= \underset{\approx}{\boldsymbol{C}} : \left(\underset{\approx}{\boldsymbol{I}} - \underset{\approx}{\boldsymbol{S}}_{L} \right) \\ \underset{\sim}{\boldsymbol{\alpha}} &= \left\langle \underset{\approx}{\boldsymbol{B}}_{L}^{g} : \underset{\approx}{\boldsymbol{C}}^{*} \right\rangle^{-1} : \left\langle \underset{\approx}{\boldsymbol{B}}_{L}^{g} : \underset{\approx}{\boldsymbol{C}}^{*} : \underset{\sim}{\boldsymbol{\alpha}}^{g} \right\rangle \end{cases} \tag{9}$$

where $\underset{\sim}{\boldsymbol{\alpha}}$ represents the overall thermal expansion tensor, $\underset{\sim}{\boldsymbol{\alpha}}^{g}$ the local thermal expansion tensor and T the temperature. The constitutive equations are then implicit, so that the numerical resolution may need intensive computations. The contributions of Kröner [13], Budiansky & Wu [33], and Weng [34] (called KBW in the sequel) consist in replacing the effective tangent operator by the effective elasticity tensor. For an anisotropic elastic behaviour at the grain scale, the KBW model conducts to the explicit transition rule given by:

$$\underset{\sim}{\boldsymbol{\sigma}}^{\mathrm{g}} = \underset{\approx}{\boldsymbol{B}}^{g} : \left[\underset{\sim}{\boldsymbol{\Sigma}} + \underset{\approx}{\boldsymbol{C}}^{*} : (\underset{\sim}{\boldsymbol{E}}^{\mathrm{p}} - \underset{\sim}{\boldsymbol{\varepsilon}}^{gp}) + \underset{\approx}{\boldsymbol{C}}^{*} : (\underset{\sim}{\boldsymbol{\alpha}} - \underset{\sim}{\boldsymbol{\alpha}}^{g})\, (T - T_0) \right] \tag{10}$$

where $\underset{\sim}{\boldsymbol{\alpha}}^{g}$ (thus $\underset{\sim}{\boldsymbol{\alpha}}$ also) does not depend on temperature for the sake of simplicity and the Eshelby tensor in $\underset{\approx}{\boldsymbol{C}}^{*}$ is associated to the effective elastic tensor $\underset{\approx}{\boldsymbol{C}}$. In the case of FCC lattice structures, the local thermal expansion is isotropic, so that the scalar value of the effective thermal expansion is equal to the local one. In such crystals, the thermal strain of a grain do not influence the others. Otherwise, the localization rule only depends on the elastic properties of both the grain g and the HEM. This model is well known to overestimate the residual stress

during plastic regime [35], leading to a too stiff global response.

Several solutions are available to introduce a softer accommodation. In the case of pure viscoplastic behaviour, a linearisation of the local behaviour was proposed by Hutchinson [36] for FCC polycrystalline aggregates, considering a power law for viscosity effects. Thereafter, more complex linearisation rules (either tangent [37, 38] or affine [39, 40]) were proposed. In all cases, the implicit form of the localisation equation ends with another iterative procedure, in order to introduce the dependence of linearised tensors to the local plastic activity of grains. Other problems concern the resolution of the general EVP problem, with the dual occurrence of time-derivative of stresses at two orders. First methods are based on the addition of a new time-integral term in the localization rule, called "long memory effect" [41, 42, 43]. These approaches are so-called hereditary. Another strategy assumes that loading path history is included within the local internal variables [44, 45]. Following this, a solution for EVP behaviour concerns the use of both asymptotic purely elastic and plastic responses (initially proposed by Kouddane *et al* [44]) and the definition of a "translated field" [46, 47]. The first model was developed using a symmetric construction based on elastic and plastic solutions. The plastic solution was first based on the secant linearisation in [46, 47] and later based on the affine linearisation in [48, 49]. A non-symmetrical approach was also proposed, considering only the viscoplastic solution, which was then "projected" in the purely elastic case [50]. This attempt provided a shorter transition rule:

$$\begin{aligned}
\dot{\underset{\sim}{\boldsymbol{\sigma}}}^{\mathrm{g}} &= \underset{\approx}{\boldsymbol{B}}^{g} : (\dot{\underset{\sim}{\boldsymbol{\Sigma}}} + \underset{\approx}{\boldsymbol{C}}^{*} : (\underset{\approx}{\boldsymbol{A}}^{g}_{L} : \dot{\underset{\sim}{\boldsymbol{E}}}^{vp} - \dot{\underset{\sim}{\boldsymbol{\varepsilon}}}^{gvp})) \\
\underset{\approx}{\boldsymbol{A}}^{g}_{L} &= [\underset{\approx}{\boldsymbol{I}} - \underset{\approx}{\boldsymbol{S}}_{L_{sec}} : (\underset{\approx}{\boldsymbol{I}} - \underset{\approx}{\boldsymbol{L}}^{eff\,-1}_{sec} : \underset{\approx}{\boldsymbol{L}}^{g}_{sec})]^{-1} \\
\underset{\approx}{\boldsymbol{C}}^{*} &= \underset{\approx}{\boldsymbol{C}} : \left(\underset{\approx}{\boldsymbol{I}} - \underset{\approx}{\boldsymbol{S}}_{L_{sec}}\right) \\
\underset{\sim}{\boldsymbol{\sigma}}^{g} &= \underset{\approx}{\boldsymbol{L}}^{g}_{sec} : \dot{\underset{\sim}{\boldsymbol{\varepsilon}}}^{gvp}
\end{aligned} \tag{11}$$

This model (marked TF in the sequel) leads to softer mechanical responses compared to KBW model [50]. Other models have been developed into the field of homogenization of polycrystalline aggregates, taking into account local field fluctuations [51, 52] or hereditary effects [39]. Another way to linearise the local mechanical behaviour was proposed by Doghri *et al* as an "incrementally affine" model [53, 54]. The idea is to construct a numerical tangent operator using the discrete form of the stress and strain tensors instead of the continuous ones

[55].

2.2. The proposed micro-mechanical model

As mentioned above, an elastic accommodation of grains (*e.g.* in the KBW model) is not good enough to represent the overall response of polycrystalline aggregates. The pragmatic solution of the β rule, first proposed by Cailletaud [14], is based on the definition of a second level of hardening at the mesoscale, reflecting plastic interactions between grains. A new set of internal variables, $\underset{\sim}{\boldsymbol{\beta}}^g$, is introduced in the localization equation. Using the non-symmetrical translated field model recalled in Eq. 12, we replace the term which represents plastic interactions ($\underset{\approx}{\boldsymbol{A}}^g_L : \dot{\underset{\sim}{\boldsymbol{E}}}^{vp} - \dot{\underset{\sim}{\boldsymbol{\varepsilon}}}^{gvp}$) by using the "intergranular" hardening variables proposed ($\dot{\underset{\sim}{\boldsymbol{\beta}}} - \dot{\underset{\sim}{\boldsymbol{\beta}}}^g$). The new scale transition rule is written (using a time integration to get an explicit form):

$$\underset{\sim}{\boldsymbol{\sigma}}^{\mathrm{g}} = \underset{\approx}{\boldsymbol{B}}^g : \left[\underset{\sim}{\boldsymbol{\Sigma}} + \underset{\approx}{\boldsymbol{C}}^* : (\underset{\sim}{\boldsymbol{\beta}} - \underset{\sim}{\boldsymbol{\beta}}^g)\right] \tag{12}$$

The rule can also be seen as an extension of Eq. 10, where the global and local plastic strain have been replaced by non-linear variables. The second order tensor $\underset{\sim}{\boldsymbol{\beta}}$ represents an effective intergranular hardening compared to the local ones $\underset{\sim}{\boldsymbol{\beta}}^g$. The model provides a pragmatic framework with a few degrees of freedom to reproduce complex interactions between grains coming from the single crystal model. Otherwise, if we start with the Hill's incremental self-consistent scheme expressed in Eq. 8, the introduction of intergranular variables may be done in two steps. First, we assume that the apparent elastic modulus of each crystal, mainly deduced from the term proportional to the global stress rate, is not affected by plasticity:

$$\underset{\approx}{\boldsymbol{B}}^{g\,-1}_L : \underset{\approx}{\boldsymbol{B}}_L \approx \underset{\approx}{\boldsymbol{B}}^{g-1} : \underset{\approx}{\boldsymbol{B}} = \underset{\approx}{\boldsymbol{B}}^{g-1} \tag{13}$$

The plastic dependency of the second term is supposed to be rewritten from $\underset{\approx}{\boldsymbol{B}}^{g\,-1}_L : \underset{\approx}{\boldsymbol{C}}^*$ to $\underset{\approx}{\boldsymbol{B}}^{g-1} : \underset{\approx}{\boldsymbol{C}}^* : \underset{\approx}{\boldsymbol{\Delta B_L}}$. In such a case, the tensor $\underset{\approx}{\boldsymbol{\Delta B_L}}$ is associated to the overall and the local plastic strain rates and replaced by the internal variables $\underset{\sim}{\boldsymbol{\beta}}$ and $\underset{\sim}{\boldsymbol{\beta}}^g$. It is worth mentioning that the first assumption could have a non-neglecting effect in the elastic-plastic transition where the internal variables $\underset{\sim}{\boldsymbol{\beta}}^g$ are not high enough to replace the softening action of $\underset{\approx}{\boldsymbol{B}}^{g\,-1}_L : \underset{\approx}{\boldsymbol{B}}_L$.

2.3. Some features around the set of internal variables $\underset{\sim}{\boldsymbol{\beta}}^g$

To enforce the condition $\langle \underset{\sim}{\boldsymbol{\sigma}}^{\mathrm{g}} \rangle = \underset{\sim}{\boldsymbol{\Sigma}}$, we found an expression of the effective intergranular hardening variable such as:

$$\underset{\sim}{\boldsymbol{\beta}} = \underset{\approx}{\boldsymbol{C}}^{*-1} : \left\langle \underset{\approx}{\boldsymbol{B}}^g : \underset{\approx}{\boldsymbol{C}}^* \underset{\sim}{\boldsymbol{\beta}}^g \right\rangle \tag{14}$$

Usually, the evolution law of the local internal variables $\underset{\sim}{\boldsymbol{\beta}}^g$ takes a form similar to one used for nonlinear kinematic hardening with one scalar parameter D [15]. But it can be extended for anisotropic materials such as DS alloys following [10]:

$$\dot{\underset{\sim}{\boldsymbol{\beta}}}^g = \dot{\underset{\sim}{\boldsymbol{\varepsilon}}}^{gvp} - \underset{\approx}{\boldsymbol{D}} : \underset{\sim}{\boldsymbol{\beta}}^g \sum_s |\dot{\gamma}^s| \tag{15}$$

The fourth order tensor $\underset{\approx}{\boldsymbol{D}}$ represents the anisotropic accommodation parameter. Other parameters can be introduced to capture the saturation of the plastic strain for non-proportional cyclic loadings (ratcheting effect) [56] or dynamic recovery effects. In the work of Sai *et al* [10], the accommodation parameter $\underset{\approx}{\boldsymbol{D}}$ has the symmetry of the HEM, which is transversely isotropic for DS materials. Since the variables $\underset{\sim}{\boldsymbol{\beta}}^g$ refer to the accommodation of the given grain g with the HEM, we suggest to express this parameter in its crystallographic coordinates. Others authors proposed to assign a different accommodation parameter for each phase [57, 58]. The FCC lattice structure of Ni-based superalloys involves a cubic symmetry for $\underset{\approx}{\boldsymbol{D}}^g$.

Another particular issue associated to DS structures is the uniform strain in the longitudinal direction, even if the loading is multi-axial. It is due to fact that grains work in parallel and have the same behaviour. Eq. 12 can be turned into:

$$\left[\underset{\approx}{\boldsymbol{I}} + \underset{\approx}{\boldsymbol{S}}_C : (\underset{\approx}{\boldsymbol{C}}^{-1} : \underset{\approx}{\boldsymbol{C}}^g - \underset{\approx}{\boldsymbol{I}}) \right] : \underset{\sim}{\boldsymbol{\varepsilon}}^{\mathrm{g},el} = \underset{\sim}{\boldsymbol{E}}^{el} + (\underset{\approx}{\boldsymbol{I}} - \underset{\approx}{\boldsymbol{S}}_C) : (\underset{\sim}{\boldsymbol{\beta}} - \underset{\sim}{\boldsymbol{\beta}}^g) \tag{16}$$

Using the Voigt notation, we can express the longitudinal strain (along $\vec{x}_3$) as follow:

$$\left[I_{3k} + S_{C3u} (\underset{\approx}{\boldsymbol{C}}^{-1} : \underset{\approx}{\boldsymbol{C}}^g - \underset{\approx}{\boldsymbol{I}})_{uk} \right] : \varepsilon_k^{g,el} = E_3^{el} + \beta_3 - \beta_3^g + S_{C3k}\beta_k - S_{C3k}\beta_k^g \tag{17}$$

For DS alloys, the Eshelby tensor has a particular form with a line of zeros (the third in this paper) to express the fact that there is no interaction between grains in the longitudinal direction. Thus, Eq. 17 can be simplified as:

$$\varepsilon_3^{g,el} = E_3^{el} + \beta_3 - \beta_3^g \tag{18}$$

One solution to get the equality between the local and overall total strains in the longitudinal direction is to introduce a line of zeros at the third position of the tensor $\underset{\approx}{\boldsymbol{D}}^g$. Doing so, the variables β_3^g are equal to ε_3^{gp} and β_3 is equal to E_3^p. With this proposition, the accommodation parameter can be represented by a matrix in the crystal coordinates, $[D^0]$:

$$[D^0] = \begin{pmatrix} D^0_{1111} & D^0_{1122} & D^0_{1122} & 0 & 0 & 0 \\ D^0_{1122} & D^0_{1111} & D^0_{1122} & 0 & 0 & 0 \\ 0 & 0 & 0 & 0 & 0 & 0 \\ 0 & 0 & 0 & D^0_{1212} & 0 & 0 \\ 0 & 0 & 0 & 0 & D^0_{1212} & 0 \\ 0 & 0 & 0 & 0 & 0 & D^0_{1212} \end{pmatrix} \tag{19}$$

As discussed by Sai *et al* [10], another condition has to be imposed on the D^0_{ijkl} to preserve the assumption of incompressibility. The authors imposed $\text{trace}(\underset{\sim}{\boldsymbol{\beta}}^g) = 0$ and found a relation between the components of the accommodation parameter (with a transverse isotropic symmetry). In our model, where the accommodation parameter is written in the crystal coordinates, it is not that easy to preserve $\text{trace}(\underset{\sim}{\boldsymbol{\beta}}^g) = 0$ for any given crystallographic orientation. But our main interest is to ensure $\text{trace}(\underset{\sim}{\boldsymbol{E}}^p) = 0$, which can be found even for $\text{trace}(\underset{\sim}{\boldsymbol{\beta}}^g) \neq 0$, as shown below. The localization rule can be written in terms of strain rates following:

$$\underset{\approx}{\boldsymbol{C}}^g : (\dot{\underset{\sim}{\boldsymbol{\varepsilon}}}^{\mathrm{g}} - \dot{\underset{\sim}{\boldsymbol{\varepsilon}}}^{\mathrm{gvp}}) = \underset{\approx}{\boldsymbol{B}}^g : \underset{\approx}{\boldsymbol{C}} : (\dot{\underset{\sim}{\boldsymbol{E}}} - \dot{\underset{\sim}{\boldsymbol{E}}}^{\mathrm{p}}) + \underset{\approx}{\boldsymbol{B}}^g : \underset{\approx}{\boldsymbol{C}}^* : (\dot{\underset{\sim}{\boldsymbol{\beta}}} - \dot{\underset{\sim}{\boldsymbol{\beta}}}^g) \tag{20}$$

Applying a volume average upon the two members of the equality, the overall plastic strain rate can be expressed as:

$$\dot{\underset{\sim}{\boldsymbol{E}}}^{\mathrm{p}} = \langle \dot{\underset{\sim}{\boldsymbol{\varepsilon}}}^{\mathrm{gvp}} \rangle + \left\langle \underset{\approx}{\boldsymbol{C}}^{g\,-1} : \underset{\approx}{\boldsymbol{B}}^g : \underset{\approx}{\boldsymbol{C}}^* : (\dot{\underset{\sim}{\boldsymbol{\beta}}} - \dot{\underset{\sim}{\boldsymbol{\beta}}}^g) \right\rangle \tag{21}$$

To prove that the trace of the plastic strain rate is equal to zero, we have to demonstrate that the second term of Eq. 21 is purely deviatoric. We can rewrite this term as follow:

$$\left\langle \underset{\approx}{\boldsymbol{C}}^{g-1} : \underset{\approx}{\boldsymbol{B}}^g : \underset{\approx}{\boldsymbol{C}}^* : (\dot{\underset{\sim}{\boldsymbol{\beta}}} - \dot{\underset{\sim}{\boldsymbol{\beta}}}^g) \right\rangle = \left\langle \underset{\approx}{\boldsymbol{S}}^g : \underset{\approx}{\boldsymbol{B}}^g \right\rangle : \underset{\approx}{\boldsymbol{C}}^* : \dot{\underset{\sim}{\boldsymbol{\beta}}} - \left\langle \underset{\approx}{\boldsymbol{S}}^g : \underset{\approx}{\boldsymbol{B}}^g : \underset{\approx}{\boldsymbol{C}}^* : \dot{\underset{\sim}{\boldsymbol{\beta}}}^g \right\rangle \tag{22}$$

By using the expression of the overall hardening variable $\underset{\sim}{\boldsymbol{\beta}}$ in Eq. 14, it comes:

$$\left\langle \underset{\approx}{\boldsymbol{S}}^g : \underset{\approx}{\boldsymbol{B}}^g \right\rangle : \underset{\approx}{\boldsymbol{C}}^* : \dot{\underset{\sim}{\boldsymbol{\beta}}} - \left\langle \underset{\approx}{\boldsymbol{S}}^g : \underset{\approx}{\boldsymbol{B}}^g : \underset{\approx}{\boldsymbol{C}}^* : \dot{\underset{\sim}{\boldsymbol{\beta}}}^g \right\rangle = \left\langle \left(\underset{\approx}{\boldsymbol{S}}^{el} - \underset{\approx}{\boldsymbol{S}}^g \right) : \underset{\approx}{\boldsymbol{B}}^g : \underset{\approx}{\boldsymbol{C}}^* : \dot{\underset{\sim}{\boldsymbol{\beta}}}^g \right\rangle \tag{23}$$

The pure deviatoric character of this term is proven by showing that the spherical part of $\underset{\approx}{\boldsymbol{S}}^{el} - \underset{\approx}{\boldsymbol{S}}^g$ vanishes. Indeed, we can write the spherical part of the local compliance tensor

as $3k_0^{-1}\underset{\approx}{\boldsymbol{K}}$ for any g because the tensor $\underset{\approx}{\boldsymbol{K}}$ is invariant. The spherical term of $\underset{\approx}{\boldsymbol{S}}^{el}$ can be transformed successively:

$$\underset{\approx}{\boldsymbol{S}}^{el} : \underset{\approx}{\boldsymbol{K}} = \left\langle \underset{\approx}{\boldsymbol{S}}^{g} : \underset{\approx}{\boldsymbol{B}}^{g} \right\rangle : \underset{\approx}{\boldsymbol{K}} = \left\langle 3k_0^{-1}\underset{\approx}{\boldsymbol{K}} : \underset{\approx}{\boldsymbol{B}}^{g} \right\rangle : \underset{\approx}{\boldsymbol{K}} = 3k_0^{-1}\underset{\approx}{\boldsymbol{K}} : \left\langle \underset{\approx}{\boldsymbol{B}}^{g} \right\rangle : \underset{\approx}{\boldsymbol{K}} = 3k_0^{-1}\underset{\approx}{\boldsymbol{K}}$$

As a consequence, the term $\underset{\approx}{\boldsymbol{S}}^{el} - \underset{\approx}{\boldsymbol{S}}^{g}$ is purely deviatoric, which ensures that there is no volume change due to plastic flow. It is worth noting that, for a hexagonal crystal, for which the local elasticity tensor also has a transverse isotropic symmetry, the result is no longer verified. The proposed model, with the accommodation parameter expressed in the crystal coordinates, authorizes a non-isochoric strain by dislocation slips. In Fig. 2, a scheme describes the micro-mechanical model proposed for DS alloys.

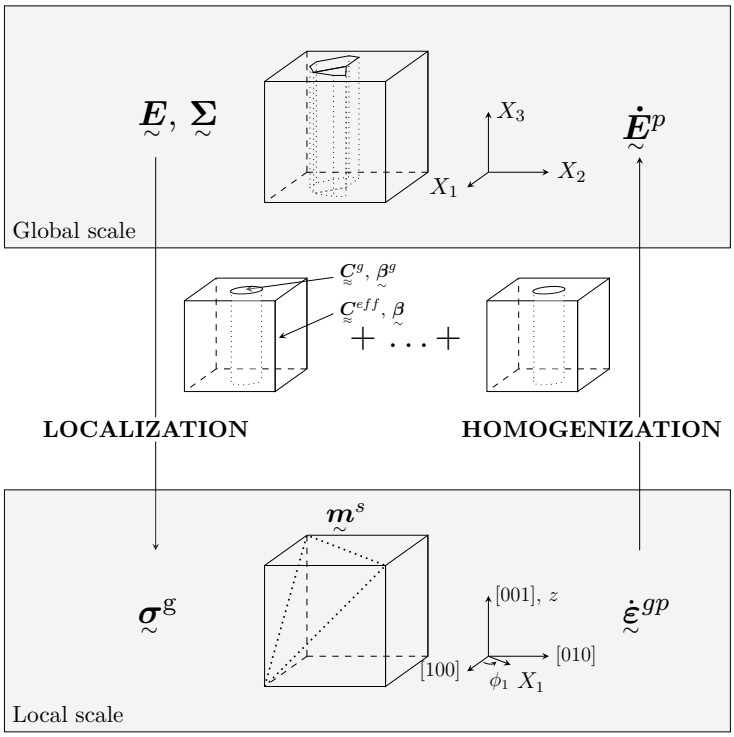

Figure 2: Multi-scale scheme for FCC polycrystalline aggregates with a directional solidification.

3. Calibration method used for β rules

As already discussed before, the β rules introduce plastic accommodations by means of phenomenological hardening variables. A new material parameter has been introduced, $\underset{\approx}{\boldsymbol{D}}^{0}$

and must be identified using either benchmark results provided by experimental tests in the transverse direction, more sophisticated mean-field models or CPFE simulations. In this paper, values for the three independent components of the accommodation parameter are searched by a comparison with CPFEM results using a representative volume element (RVE) of the material.

3.1. Definition of the RVE

This first part is devoted to the definition of a RVE for DS alloys. First, a Voronoï tesselation has been used to generate a square of a periodic synthetic aggregate in the plane (x_1, x_2) (schematized in the "Global scale" rectangle of Fig. 2). This surface was extended in the x_3 direction to provide a perfect columnar structure as assumed ideally for this kind of material (mesh of synthetic aggregates are presented in Fig. 3). In addition, a periodic mesh was achieved to get coincident nodes between two opposite faces, edges and corners. This was generated using the Z-set code [59] (developed by Mines ParisTech and ONERA) with the module called *vpoly3d* [60]. For pure tensile or shear tests in the transverse direction, the strain along x_3 axis remains uniform, allowing the use of one element for this kind of loading. However, for shear tests with components E_{31} or E_{23}, several elements may be added in the thickness. Fig.3 shows the strategy of computations which is achieved for each loading investigated.

First, we assign different set of crystallographic orientations to each group of elements depicting a grain. Due to the symmetry of FCC crystal and the texture of DS materials, only one Euler angle is used and chosen between 31 different orientations from $\phi_1 = 0°$ to $\phi_1 = 90°$ (i.e $\in \{0°, 3°, ..., 87°, 90°\}$). These crystallographic orientations are randomly assigned to the 256 grains of the cubic cell, respecting the "grain continuity" on the edges of the volume (the same colour is found for the two parts of grains cut by an edge in Fig. 3. The combination of the periodic mesh and one set of orientations represents one CPFE realization. To define rigorously the RVE, we have to introduce a sufficient number of grains within the volume to get stable effective properties if its size is extended. In [61], the authors proposed to enlarge the definition of a RVE to smaller volume, adding several realizations and making a volume average. In this paper, the size of the volume is fixed and the number of realizations is defined in order to access overall quantities with a given relative errors (less than 1 % for the presented results).

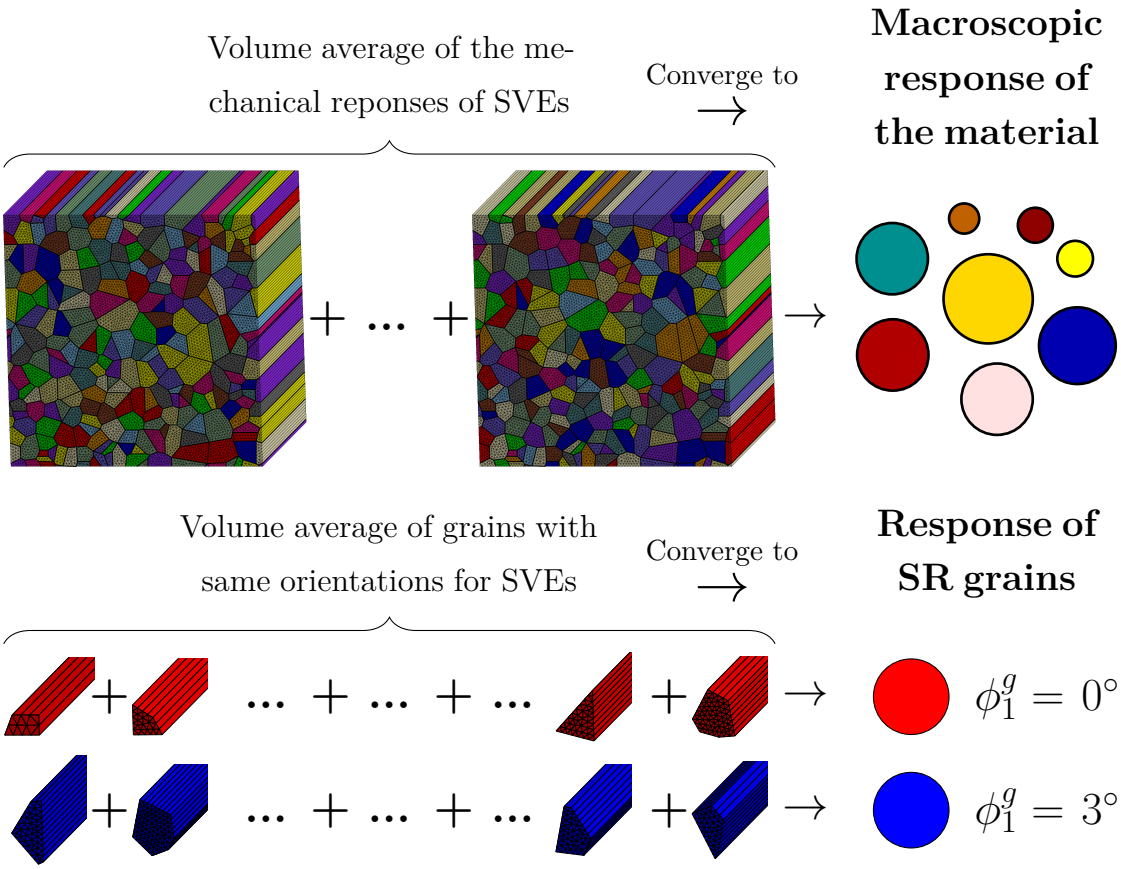

Figure 3: Strategy of computations used to calibrate the accommodation parameter of the β model, which is composed of (i) several CPFE computations on a periodic synthetic DS aggregate seen as a Statistical Volume Element (SVE) (ii) a volume average of the stress and strain components to access the effective behaviour and (iii) a volume average of stress and strain for grains with the same crystallographic orientation to access local estimations for statistically representative (SR) grains.

Otherwise, mean-field models give also access to average quantities per crystallographic phase (*e.g.* $\underset{\sim}{\boldsymbol{\sigma}}^{\mathrm{g}}$, $\underset{\sim}{\boldsymbol{\varepsilon}}^{\mathrm{g}}$, ...). In this paper, we try to define similar quantities in the case of a full-field modeling. Doing so, all the data collected from the number of CPFEM realizations are sorted in order to make volume averages of grains with the same crytallographic orientation but different shapes and neighbours (see the Fig. 3).

3.2. Single crystal behaviour

The parameters of the single crystal model (the same for full-field and mean-field simulations) are calibrated with the experimental tests in the longitudinal direction of a DS Ni-based superalloy found in [8] (see Fig. 4). Assuming that all the grains share their $\langle 001 \rangle$ crystallographic axes, there is no intergranular residual stresses, and the overall response of the β model is exactly the same as the single crystal in this crystallographic direction.

C_{1111} [MPa]	C_{1122} [MPa]	C_{1212} [MPa]
190207	110773	118500
K [MPa.s$^{1/n}$]	n	τ^{c} [MPa]
150	16	240
Q [MPa]	b	C [MPa]
30	100	100000
D		
5000		

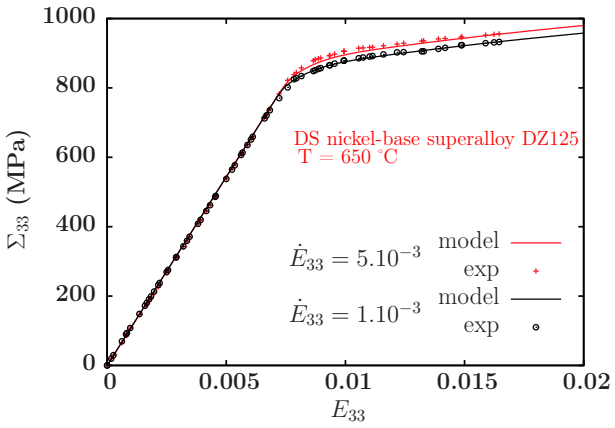

Figure 4: Tensile curves in the longitudinal (x_3) direction for the DS superalloy DZ125 at 650 °C for two strain rates. There is a good agreement between the experimental data [8] and the response of the model (DS and single crystal models give thei same curves).

The next part deals with the calibration of the accommodation tensor $\underset{\approx}{\boldsymbol{D}}^{0}$ using a full field modeling (called "FF model" in the sequel) with the local behaviour identified.

3.3. Uniaxial transverse tensile test

A transverse tensile test is performed in the direction $\vec{x}_1$. The macroscopical strain $E_{11} = 0.02$ is imposed with a constant rate $\dot{E}_{11} = 10^{-5}\mathrm{s}^{-1}$. All the components of the overall

stress tensor $\underset{\sim}{\mathbf{\Sigma}}$, except Σ_{11}, remain equal to zero. The effect of the viscosity can be quantified using an upper bound (uniform strain) following $\Sigma_v = K(\dot{E}_{11})^{\frac{1}{n}}$. In the present case, the viscous effect is limited in comparison to the yield stress ($\Sigma_v = 73\,\text{MPa}$). The map of the axial strain ε_{11} at the end of the loading and the effective responses for both the full field (FF) model and the three MF models are plotted in Fig. 5.

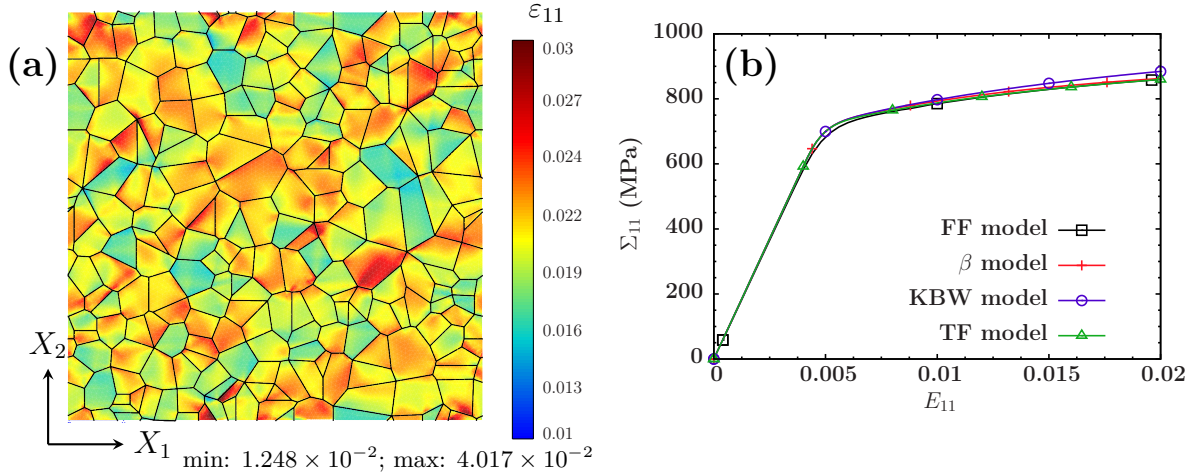

Figure 5: Map of the transverse axial component of the strain tensor at the end of the loading and the overall response for both FF and MF models during an uniaxial transverse tensile test in the $\vec{x}_1$ direction.

We can observe a heterogeneous strain field in Fig. 5.a, with local values fifty percent higher or smaller than the overall strain. Otherwise, the continuity of the strain around the border of the volume is preserved, as allowed by the periodic boundary conditions. The overall stresses computed by both the translated field model and the β rule are in good agreement with the FF model. As well commented in the literature, a purely elastic accommodation of grains yields to an overestimate of the stress for large plastic strains. Even if these results at the macroscopic scale are well known, the consistency of local estimations provided by micro-mechanical models ($\underset{\sim}{\boldsymbol{\sigma}}^g$, $\underset{\sim}{\boldsymbol{\varepsilon}}^{\mathrm{g}}$) and used to compute the overall behaviour are not often studied. In this study, a procedure was developed to evaluate these quantities. They are obtained by a volume average of numerous "avatars" (grains with a given orientation but different shapes and neighbourhoods). The averaging process allows to reach the behaviour of a cylindrical grain in an homogenized matrix, meeting the conditions of the self-consistent scheme. Even for a one-dimensional macroscopic load, the local stress state is no longer

one-dimensional at the local scale (see Fig. 6).

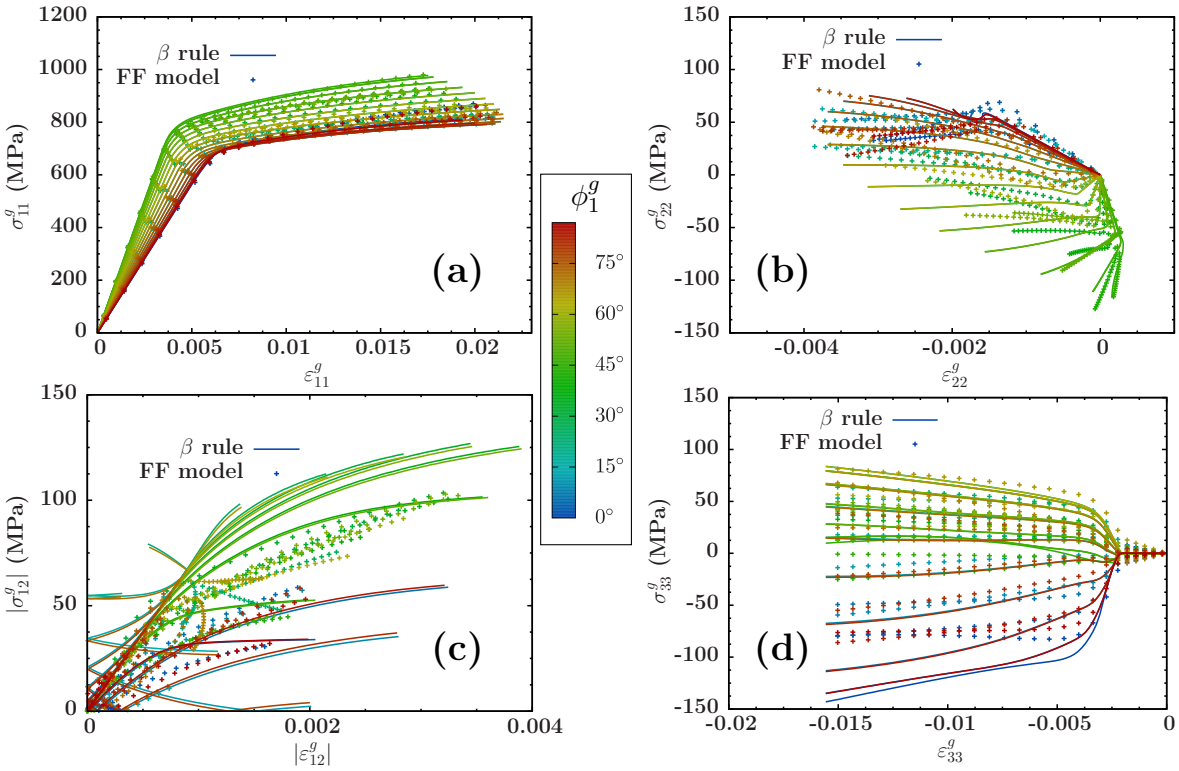

Figure 6: Local "per phase" average responses of an uniaxial transverse tensile loading in the $\vec{x}_1$ direction for the FF model (dotted curves) and the β model (full lines) (the color code refers to the orientation of the crystallographic phase).

The uniaxial transverse tensile test is mainly used to adjust the value of D^0_{1111}. This parameter control the overall hardening slope and the release of the residual stresses due to plasticity. In a second step, the value of D^0_{1212} must be checked, since coupling effects appear (Fig. 6) between the applied tensile loading and plastic flow for the shear component ε^{gp}_{12}. The key issue when analyzing local responses of the β rule with FF model is to converge to an optimal accommodation tensor with a low number of cases. For the evolution of local responses with respect to their crystallographic orientations, a symmetry is found for an orientation ϕ_1 and $90 - \phi_1$. The local responses for the 11 and 12 components are plotted for both the TF model and the KBW model in Fig. 7.

For the KBW model, the accommodation slope is linear, as well known in the isotropic

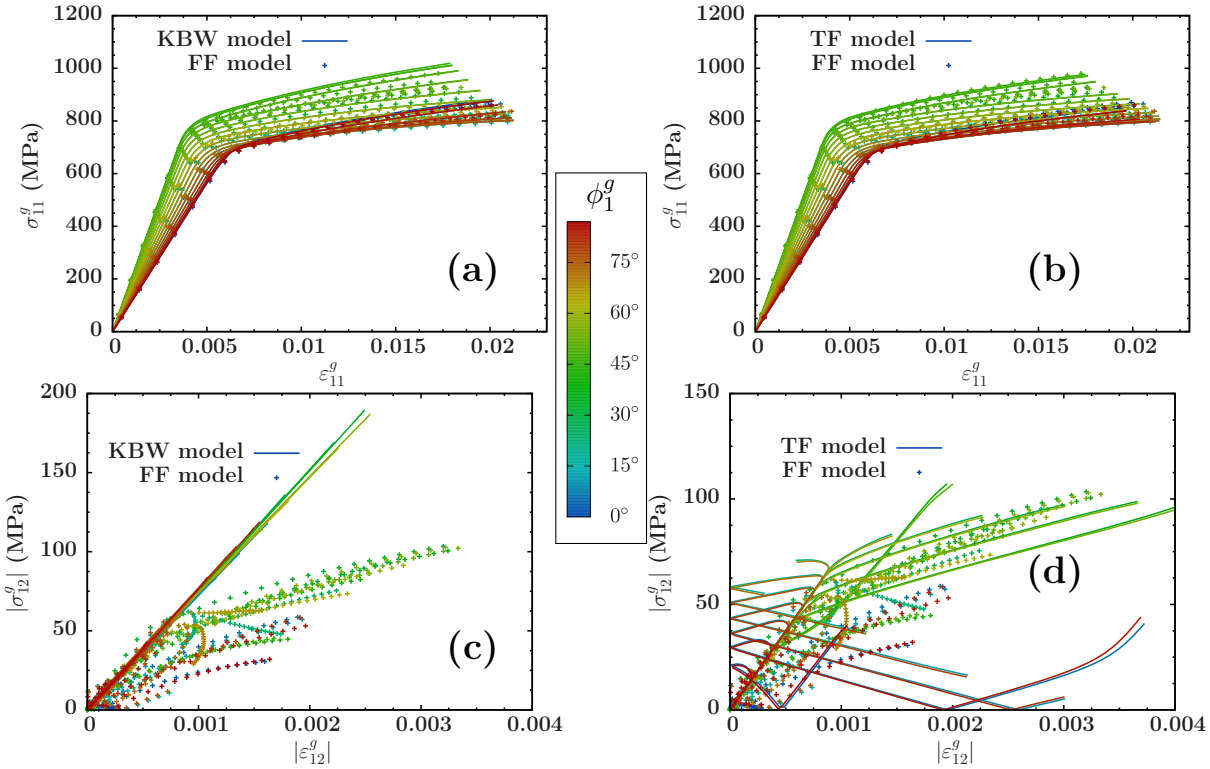

Figure 7: Local "per phase" average responses of an uniaxial transverse tensile loading in the $\vec{x}_1$ direction for the FF model (dotted curves) and the TF and KBW models (full lines) (the color code refers to the orientation of the crystallographic phase).

case and equal to the shear coefficient μ if $\nu = 0.33$. Otherwise, considering only an elastic accommodation prevents the formation of a shear plastic flow ($\dot{\varepsilon}^{gp}_{12} = 0$). And that is due to the tensile/shear components of the effective elastic tensor which are equal to zero. For the TF model, the local estimations are quite similar to those provided by the β rule. During plastic flow, the slope of hardening in the plan (ε_{12}, σ_{12}) is in good agreement with the FF model. However, the plastic strain is overestimated for crystal orientations close to ϕ_1=0°. It is worth mentioning that the evolution of the stress and strain (in terms of absolute value) for these kinds of crystal orientation is unusual, with a decrease of the stress and strain levels after the onset of plasticity.

To quantify more precisely the local errors attached to each homogenization technique, the final values of σ^g_{11} and ε^g_{11} are plotted against FF results for each orientation (see Fig. 9,(a) and (b)). The maximal error on the local stresses for the three MF models is less than 5 %. Regarding the local strains, the values estimated by the β rule are not satisfactory for crystallographic phases with $\phi_1 \in \{0°, 3°, 87°\}$. We chose a value of the parameter D^0_{1212} which does not provide optimal results for this kind of test but a compromise with the results of pure shear loading.

As discussed in section 2, the rate dependency of the behaviour adds new complexities in the definition of a scale transition rule. Among the three models compared, KBW does not account for VP effects in the stress redistribution, the β rule takes into account plasticity by a phenomenological way but *a priori* not the viscosity whereas the translated field model is developed using the general EVP framework. It may then be useful to understood how these different natures affect the mechanical predictions. To elucidate this point, the strain rate is increased to 10^{-4}s^{-1} and the two parameters used to define the flow rule K, n are turned respectively into 2000 MPa.s$^{1/n}$ and 4 (called the "HV" parameters). The color map of the total axial strain at the end of the loading and the effective responses of the models are plotted in Fig. 8.

The observation shows that MF models, independently from their transition rule, provide an overall response close to the FF model. Regarding local estimations, the viscosity seems to be beneficial since the errors on local stresses and strains with respect to FF are smaller with a

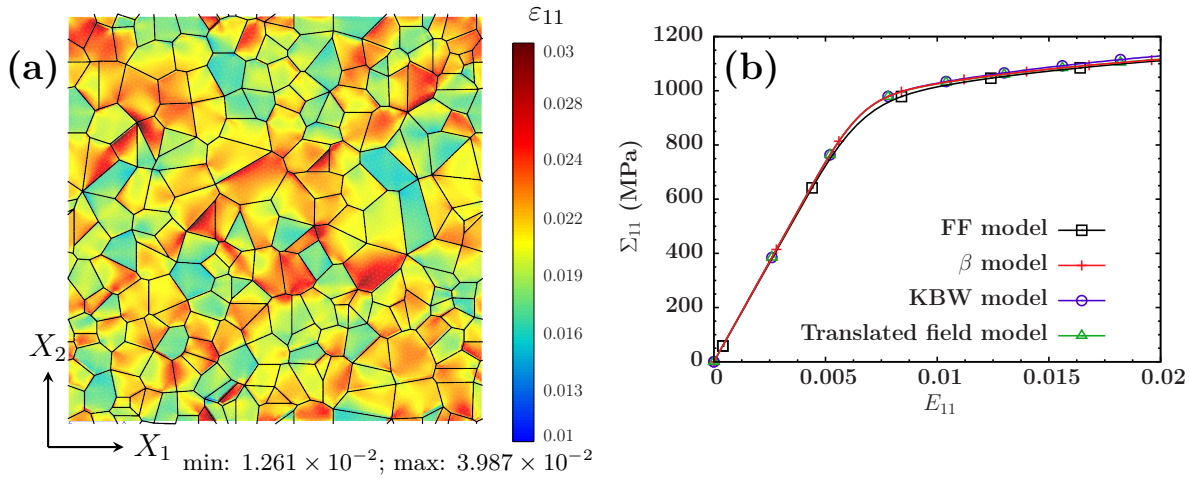

Figure 8: Map of the transverse axial component of the strain tensor at the end of the loading and the overall response for both FF and MF models during an uniaxial transverse tensile test in the $\vec{x}_1$ direction (with the HV parameters).

large viscosity than for the low viscosity case (see Fig. 9,(c) and (d)). It might be associated to the decrease of the anisotropy of single crystal Ni-based superalloys at high temperature (and where viscous effects are predominant) [62, 63, 64].

Regarding the local stresses, even though the values are higher for the HV parameters, the differences between the MF models and the FF model seem to meet the case with low viscosity (LV) parameters. All results provided by each MF model with the HV parameters are included within the $\pm 5\%$ error bars. Nevertheless, the influence of the crystallographic orientation on the local strains is not the same for the LV and the HV parameters. In the LV case, the local strain increases when the Euler angle ϕ_1 increases up to approximately 15°. Then, the local strain decreases when ϕ_1 increases until 45°. In the case of HV parameters, the local strain is quasi stable for crystallographic orientations between 0° and 15° and equal to 2.1 %.

3.4. One-dimensional transverse shear test

The other test case used to calibrate the components of the tensor $\underset{\approx}{\boldsymbol{D}}^0$ is a pure transverse shear loading. For this, an overall strain $E_{12} = 0.02$ is applied, with a constant strain rate $\dot{E}_{12} = 10^{-5}\text{s}^{-1}$. As done for the previous loading case, all the components of the stress tensor, except Σ_{12}, are imposed equal to zero. The effective response for both FF and MF models are plotted in Fig. 10.

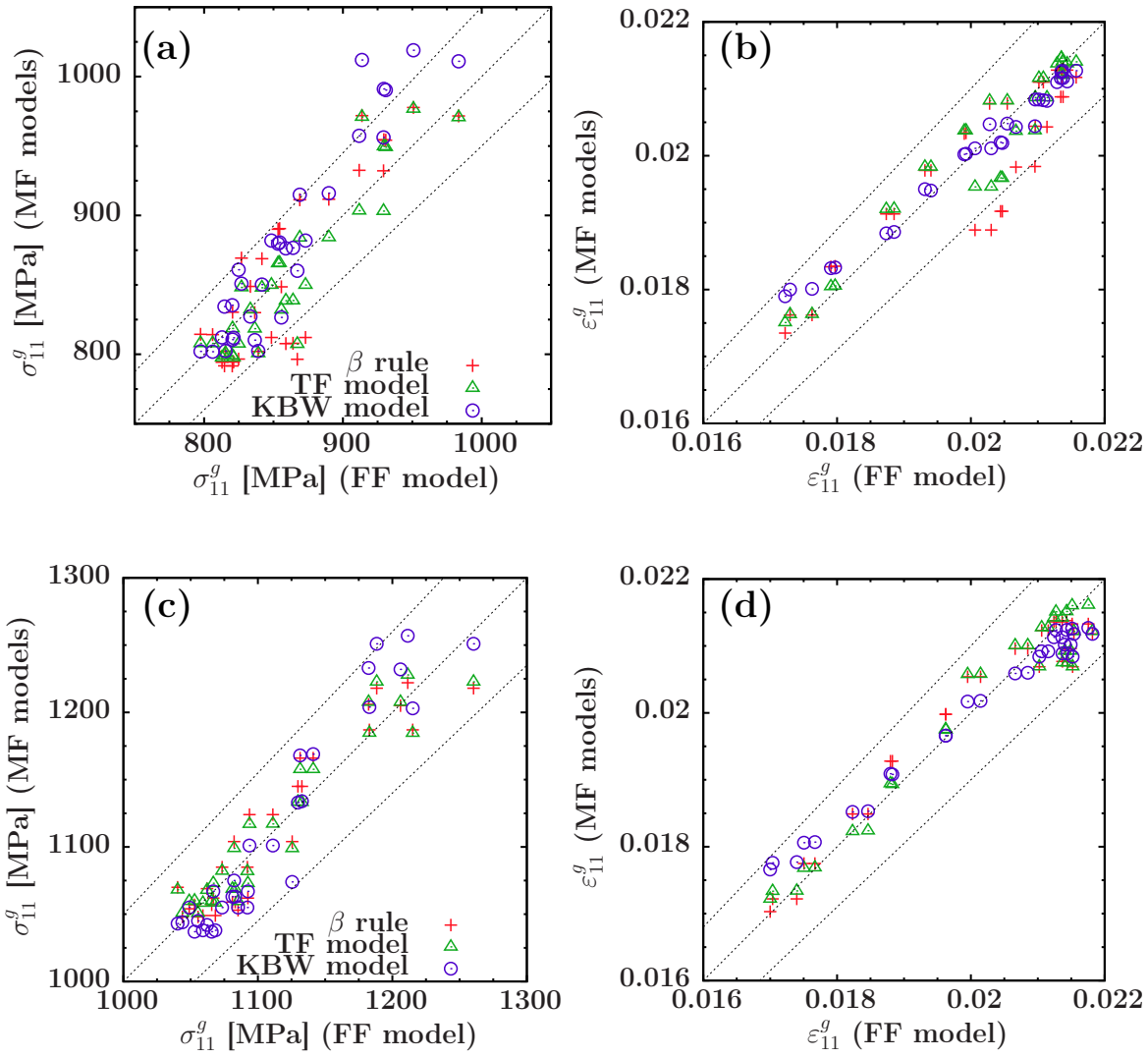

Figure 9: Comparative results on the final values of the local stress component σ^g_{11} (a) and (c) and the local strain component ε^g_{11} (b) and (d) for each MF model and the FF model with a "low viscosity (LV)" (a) and (b) or a "high viscosity (HV)" (c) and (d). Black dotted lines represent $\pm 5\%$.

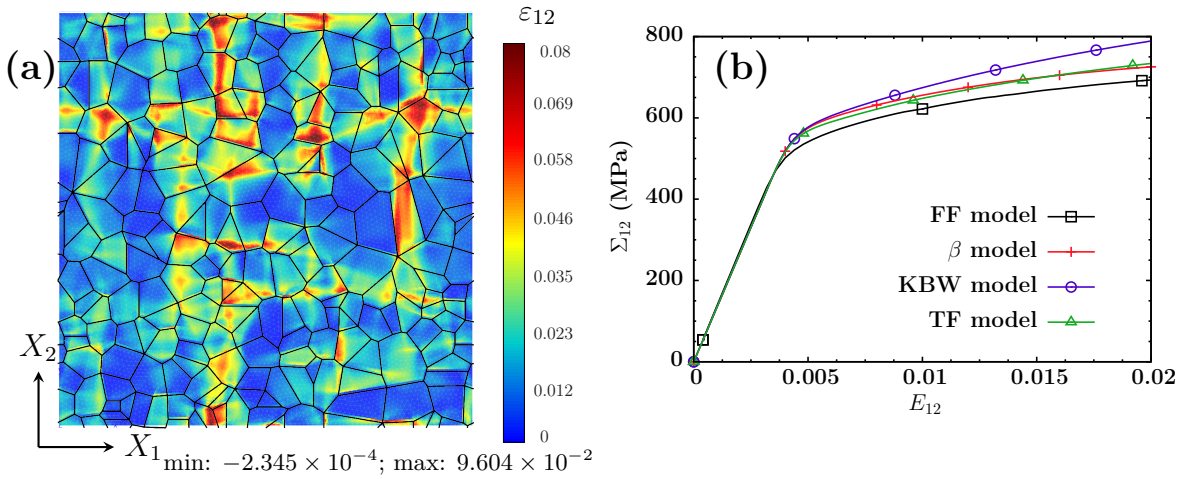

Figure 10: Map of the transverse shear component of the strain tensor at the end of the loading and the overall response for both FF and MF models during an uniaxial transverse shear test in the plane X_1/X_2.

The phenomenological form of the plastic accommodation into the β rule gives the opportunity to access to a softer overall response than TF and KBW models. The values of the three parameters used for the calibration of $\underset{\sim}{\dot{\boldsymbol{\beta}}}^g$ can be found in Tab.1.

	D^0_{1111}	D^0_{1122}	D^0_{1212}
Low viscosity	180	80	100
High viscosity	130	40	70

Table 1: Values of tensor $\underset{\approx}{\boldsymbol{D}}^0$ for high and low viscosity cases

Otherwise, the three MF models are not able to track precisely the yield stress observed on the FF results. This conducts to overestimate the global stress for low plastic strain amplitude. The β rule allows artificially to merge the FF response when the strain still increases, thanks to the intergranular hardening. However, when "per phase" local responses are compared for FF and MF models (see Fig. 11), the yield stresses of the first grains becoming plastically activated ($\phi_1 \in \{39°, 42°, 45°, 48°, 51°\}$) are very similar to FF predictions.

The problem seems to be elsewhere, maybe into the modification of the purely elastic behaviour of others grains. This can be highlighted by plotting the final errors for MF local stresses compared to FF ones (see Fig. 12,(a)). The linear slope predicted by the KBW model for the intergranular accommodation is too stiff. By consequence, the final values of the local

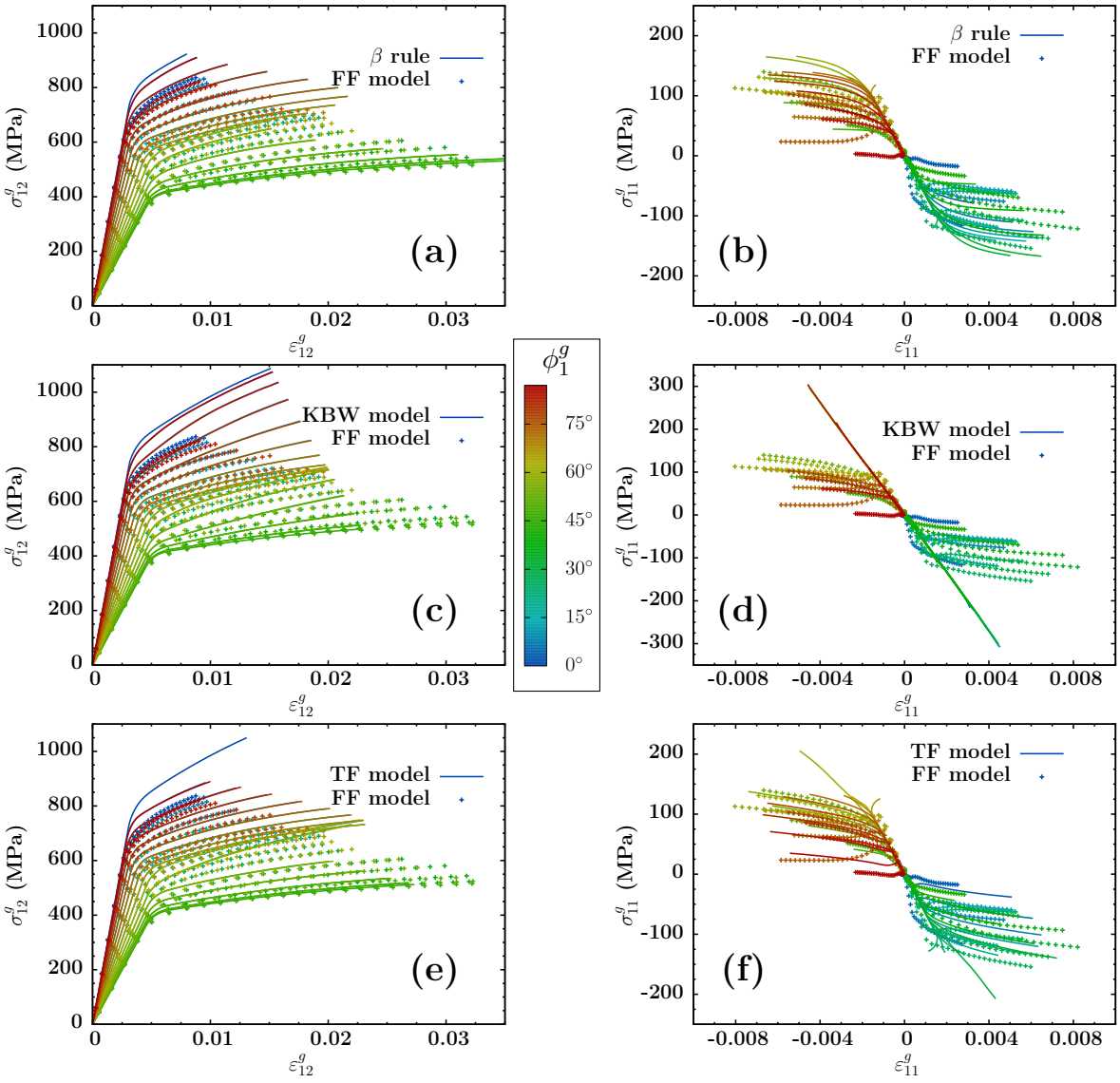

Figure 11: Local responses averaged on 12 CPFE simulations and estimated by each MF model during an uniaxial shear loading: (a,b) for the β rule, (c,d) for the KBW model and (e,f) for the translated field model.

strain for close [110]-oriented grains and [100]-oriented grains are respectively underestimated or overestimated (see Fig. 12,b.). For the other local nonzero components ("11" and "22") of the stress and strain tensors, the β rule and the TF models provide good estimations. As discussed before, the KBW model is not able to predict the coupling due to the interaction between tensile and shear components of the plastic strain rate.

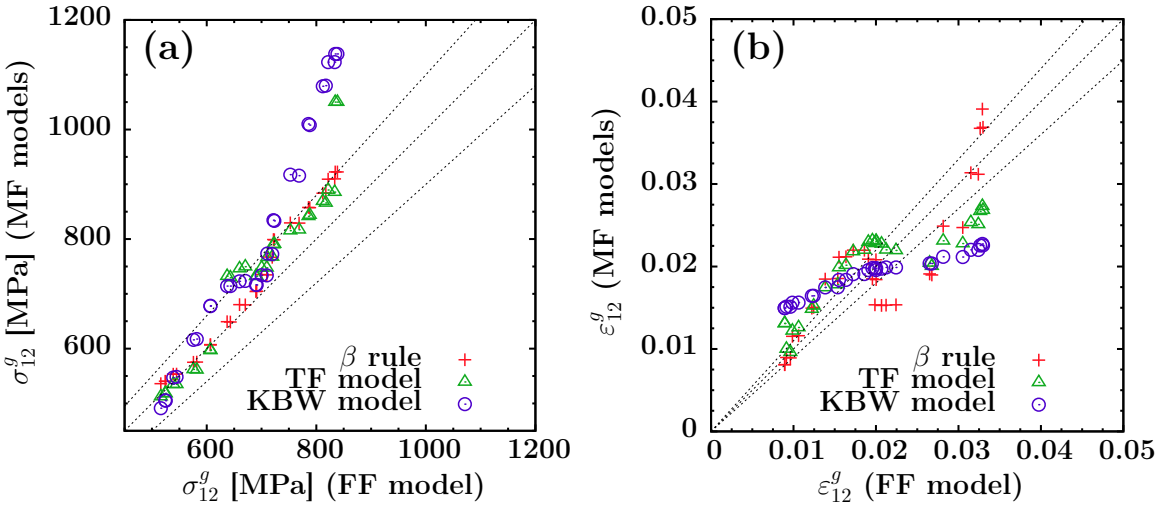

Figure 12: Comparison of the final value of the local stress (a) and the local strain (b) component $\varepsilon^g_{12}/\sigma^g_{12}$ for each MF model with FF responses.

To conclude this section, the calibration of the β rule was done using two uniaxial loading paths in the transverse direction (tensile and shear). But if we use local estimations in the identification process, we may have enough information to obtain a unique and optimal $\underset{\approx}{\boldsymbol{D}}^0$. The modification of the β model proposed in this paper provides decent results in comparison to the KBW model and the translated field model. It seems to be a good compromise between the precision of the mechanical response and the CPU cost, five times lowest for the β rule than for the translated field model for a transverse tensile test. Otherwise, some drawbacks, like the interaction between plastically activated grains and those which are not, still generate overestimations on the effective stress in some cases. Finally, it is worth noting that assuming a perfect DS microstructure induces a uniform mechanical response of the aggregate when a pure longitudinal tensile test is applied (*i.e.* a tensile loading applied parallel to the axis of cylindrical grains), so that we can use longitudinal experimental tests on DS alloys to identify

the single crystal behaviour of grains.

4. Investigation of unidimensional and two-dimensional cyclic loadings

In this section, more complex tests are investigated. The main purpose is to check the capabilities of the β rule, when other phenomena such as cyclic ratchetting are considered.

4.1. One-dimensional transverse tensile test with a cyclic strain ratio $R_\varepsilon = -1$

The boundary conditions imposed are the same as for the monotonic loading cases used in 3.2. Only five cycles are calculated because the steady state is rapidly reached, due to the value of the parameter b ($b = 100$). In addition, the value of the cyclic hardening is low (Q=30 MPa). Results in Fig. 13.(a) show good agreement between the β rule and the FF model for the first and the stabilized cycle. The comparative procedure was also made with a higher local isotropic hardening. In such a case, the asymptotic stress induced by cyclic hardening is increased to $Q = 200$ MPa (the other parameter b is turned to 10). Then, the behaviour obtained is no longer associated to a real material and is only used to show the ability of MF model to represent other phenomena such as cyclic hardening or ratchetting. Without modifying the other constants, there is a rather good correlation between the two models for the effective quantities (see Fig. 13.b).

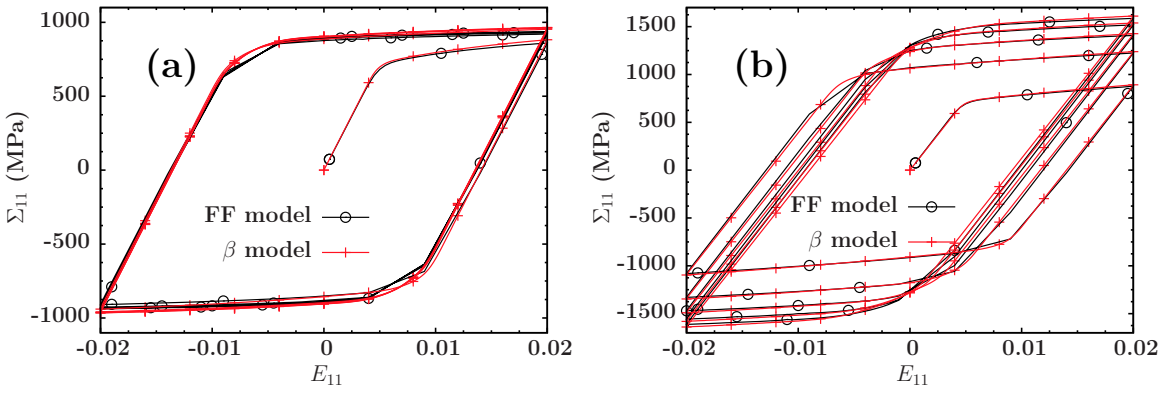

Figure 13: Effective response with both FF and MF models for a one-dimensional transverse tensile load with a cyclic strain ratio $R_\varepsilon = -1$ with (a) low isotropic hardening effects and (b) high isotropic hardening effects.

As done during the identification procedure, the local responses of the models have also been studied, and particularly for this test case, the evolution of the cyclic hardening for each crystallographic phase. Fig. 14 shows the evolution of the "per phase" local stress and strain values at the end of both load and unload parts of each cycle.

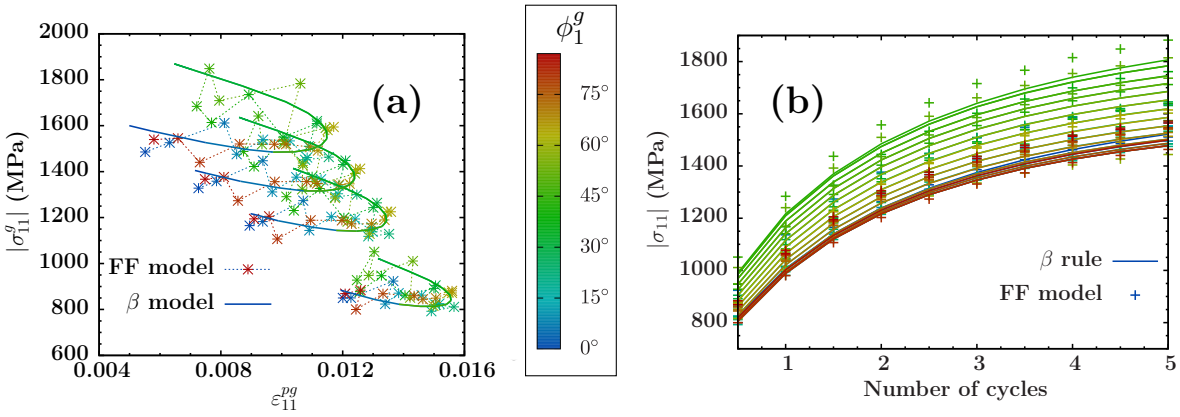

Figure 14: Evolution of the absolute value of the local plastic strain and the local stress at the end of each load and unload cycle. (a) Location of the extrema in the ε_{11}^{pg}-$|\sigma_{11}^g|$ plan, with points for the FF model, and lines as envelopes of the β model points. (b) Evolution of the hardening versus the number of cycles

The β rule is able to predict the stress hardening during cycles. Moreover, it appears that the positions of each crystallographic phase in the local stress distribution remain stable. The form of the curves composed of each local values at a given time does not vary significantly and may be only amplified by a growth of the global stress.

4.2. One-dimensional transverse tensile test with a cyclic stress ratio $R_\sigma = -0.5$

Non-proportional cyclic loads allow investigating a well known effect called cyclic "ratchetting". This phenomenon has been extensively studied for various kind of metallic aggregates [65, 66, 67]. A review of several modeling strategies can be found in [68]. In the case of the β rule, the ratchetting effect has been already well studied in [69]. A specific parameter was introduced, in order to control the plastic strain increment along cycles. Otherwise, Saï & Cailletaud studied the impact of the form of intergranular and intragranular hardening on the evolution of ratchetting [70]. When the intergranular kinematic hardening (*i.e.* the evolution of the set of variables $\underset{\sim}{\boldsymbol{\beta}}^g$) is kept nonlinear, authors showed that it is the value of the local

kinematic hardening parameter d which has a prominent effect on ratchetting. If $d = 0$ (the local kinematic hardening is linear), shakedown occurred. Otherwise, a ratchetting effect is observed. In this part, the idea is to compare the prediction of the β rule with full-field results with $d \neq 0$. The main difference between the previous comparisons and the present study is the introduction of elastic heterogeneity.

For the FF model, a periodic reaction force is applied in the transverse direction. The maximum and minimum stress values are respectively 820 MPa and -410 MPa. If the material parameters fitted on the experimental results of Dong *et al* are used [8], we observe closed loops in compression in the effective stress and strain space (see Fig. 15(a)). This is not exactly ratchetting, but a creep effect, mainly controlled by viscosity. In such cases, the accumulated plastic strain tends to saturate after some cycles. The β rule provides an evolution of the effective axial strain close to the results of the FF model. The yield surface translation is not big enough, so that there is no plastic strain during unloading. In this way, the same work was carried out with a lowest value of the parameter $d = 100$ (see Fig. 15(b)), and the ratchetting phenomenon is then observed.

The effective response predicted by the MF model is in good agreement with the FF model. After ten cycles, there is a short decrease in the value of the increment of axial strain. For more accuracy, a specific shape could be used for the variables $\underset{\sim}{\boldsymbol{\beta}}^g$, but it does not seem mandatory in the present case.

4.3. Two-dimensional transverse tension/shear loading

As seen in the previous section, the β model but also the other mean-field models studied in this paper overestimate the overall stress during transverse shear loading. Otherwise, during cyclic tests with a mean stress (which generates ratchetting), the mistaken values of the stress and strain made tend to be magnified after several loops. In this part, a two-dimensional cyclic path is achieved. A tensile mean-stress is first imposed to the material with a value Σ_{11}=1000 MPa, so that the macroscopic yield stress is exceeded. While maintaining this constant mean-stress, a cyclic shear loading in the transverse direction is carried out with a strain ratio $R_\varepsilon = -1$ and with a shear strain amplitude of 0.04. It is well known that this kind of test may generate an accumulation of inelastic strain in the axial direction. Results

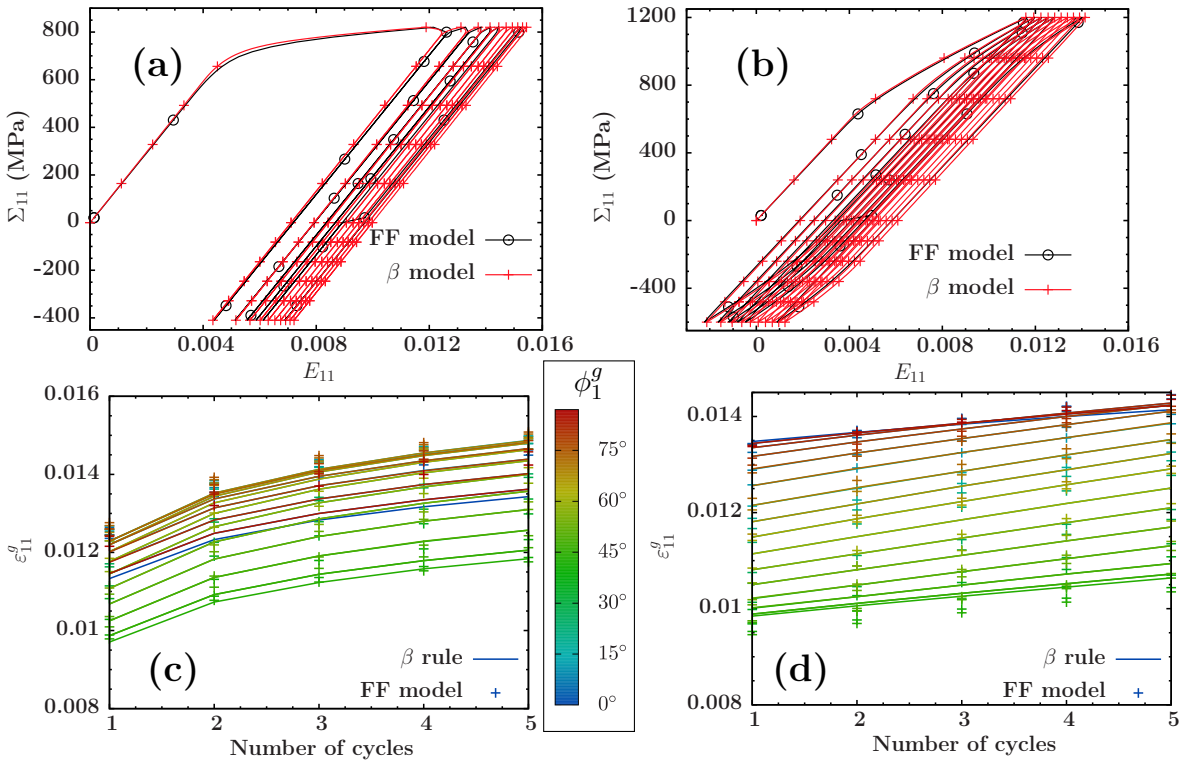

Figure 15: Effective response (a,b) and accumulated strain for each crystallographic phase of both FF and β models for a one-dimensional transverse tensile load with a cyclic stress ratio $R_\sigma = -0.5$ with (a,c) high kinematic hardening parameter $d = 5000$ and (b,d) low kinematic hardening parameter $d = 100$.

for the FF model and the β rule in the tensile-shear strain plan are plotted in Fig. 16.a. In Fig. 16.b, the accumulated axial strains for each phase is represented along cycles. We use the local kinematic hardening parameter d which generates ratchetting.

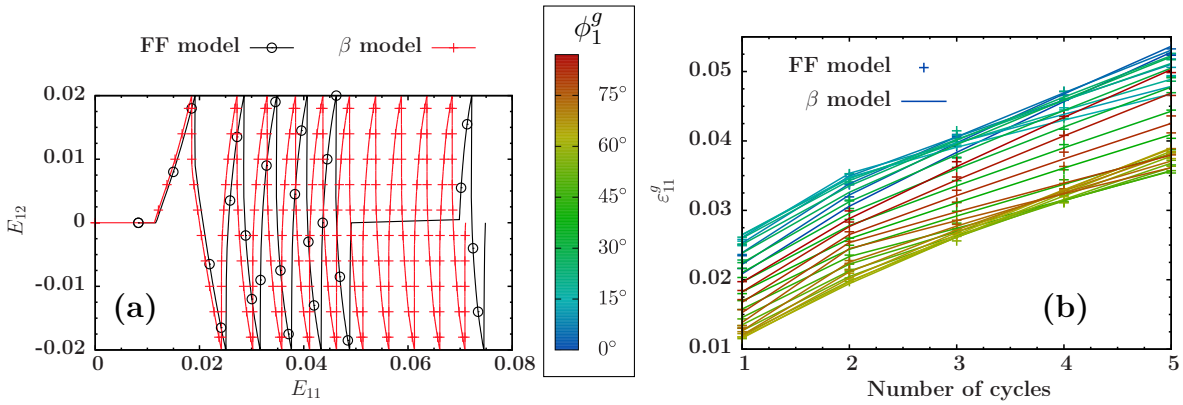

Figure 16: (a) Overall response and (b) local responses averaged on 12 CPFE simulations and estimated by the β model for a two-dimensional transverse tensile/shear loading with a mean-stress and a shear strain ratio $R_\varepsilon = -1$.

At each cycle, the β rule predicts a higher value of the accumulated axial strain. This difference is added along cycles and becomes non-negligible after ten cycles (see Fig. 16.a). Another interesting feature is the evolution of the accumulated axial strain with respect to crystal orientations, plotted in Fig. 16.b. At the first point $E_{12} = 0.02$, the maximum and minimum axial strains are localized for respectively $\phi_1 = 18°$ and $\phi_1 = 63°$ (*i.e.* $+45°$ toward the extreme values). A same distribution of the axial local strains was observed for an uniaxial shear test (see Fig. 11). Along cycles, the "per phase" accumulated axial strains have different slopes with respect to their crystallographic orientation. After five cycles, the largest axial strain is obtained for $\phi_1 = 0°$ and the lowest value for $\phi_1 = 45°$. Such a distribution is more in accordance with an uniaxial tensile test (see Fig. 11).

5. Concluding remarks and further works

In this study, the so-called β rule applied to a polycrystalline plasticity model was extended to the general case of heterogeneous local elasticity tensors. For directionally solidified alloys, we have proposed an evolution for the internal variables $\underset{\sim}{\beta}^g$ by using an accommodation parameter written in the crystal coordinates, a cubic symmetry and a line of zeros in the

longitudinal direction such as the Eshelby tensor. In a second part, the accuracy of the proposed model was quantified in comparison with two models of the literature. A reference response was constructed by means of several CPFE simulations using a volume element. The "intergranular hardening" parameter, $\underset{\approx}{\boldsymbol{D}}^0$, is first calibrated to fit the global response and "per phase" estimates given by the FF model for uniaxial tests. We have observed a well known features of the KBW model which clearly overestimated the global response during an uniaxial shear loading and, to a lesser extent, for an uniaxial tensile loading. Another issue of a purely elastic accommodation was the uncoupling in the plastic flow between tensile and shear components. Otherwise, the β model developed provided rather good local estimations compared to more complex "mean-field" models such as the Translated Field approach. In this paper, we have worked towards a better understanding of the mechanical responses of models at the scale of crystallographic phases. First, this kind of study was useful to find optimal values for the accommodation parameter introduced into the β rule without a large number of cases. Secondly, the results of some mean-field models are consistent, in the evolution of stress and strain with respect to crystallographic orientation but also in the final values, with full-field simulations. It is worth noting that the upper and lower bounds of these local responses can be equal to $\pm 10\%$ for a uniaxial tensile test and can be reached $\pm 20\%$ for a shear loading. Such values appear non-negligible when life prediction is investigated. As a consequence, it may be useful to design components with the knowledge of this average scatter, particularly for directionally solidified superalloys where the size of grains may be really large compared to the dimensions of the structure. With the improved performance of data processing, a structural computation with this kind of model, which involves a very large number of internal variables, is now accessible. Thus, only one simulation gives us an access to a more precise overall response, but also a first idea of how a given crystallographic orientation could control the mechanical response of each zone of a 3D component.

References

[1] D. Shi, J. Liu, X. Yang, H. Qi, J. Wang, Experimental investigation on low cycle fatigue and creep–fatigue interaction of dz125 in different dwell time at elevated temperatures, Materials Science and Engineering A 528 (1) (2010) 233 – 238, special Topic Section: Local and Near Surface Structure from Diffraction.

[2] X. He, Y. Zhang, H. Shi, J. Gu, C. Li, K. Kadau, O. Luesebrink, Influence of orientation and temperature on the fatigue crack growth of a nickel-based directionally solidified superalloy, Materials Science and Engineering A 618 (2014) 153 – 160.

[3] R. Kashinga, L. Zhao, V. Silberschmidt, F. Farukh, N. Barnard, M. Whittaker, D. Proprentner, B. Shollock, G. McColvin, Low cycle fatigue of a directionally solidified nickel-based superalloy: Testing, characterisation and modelling, Materials Science and Engineering A 708 (2017) 503 – 513.

[4] R. C. Reed, The superalloys: Fundamentals and Applications, Cambridge University Press, 2006.

[5] L. Mataveli Suave, High Temperature Durability of DS200+Hf Alloy, phdthesis, ISAE-ENSMA Ecole Nationale Supérieure de Mécanique et d'Aérotechique - Poitiers (2017).
URL `https://tel.archives-ouvertes.fr/tel-01735231/document`

[6] M. Shenoy, D. McDowell, R. Neu, Transversely isotropic viscoplasticity model for a directionally solidified Ni-base superalloy, Int. J. of Plasticity 22 (2006) 2301–2326.

[7] M. Yaguchi, Anisotropic viscoplasticity constitutive model for directionally solidified superalloy, Materials at High Temperatures 29 (2012) 308–314.

[8] C. Dong, X. Yang, D. Shi, H. Yu, Modeling of anisotropic tensile and cyclic viscoplastic behavior of a nickel-base directionally solidified superalloy, Materials and Design 55 (2013) 966–978.

[9] M. Yaguchi, E. Busso, On the accuracy of self-consistent elasticity formulations for directionally solidified polycrystal aggregates, Int. J. Sol. Structures 42 (2005) 1073–1089.

[10] K. Sai, G. Cailletaud, S. Forest, Micro-mechanical modeling of the inelastic behavior of directionally solidified materials, Mech. of Materials 38 (2006) 203–217.

[11] G. Taylor, Plastic strain in metals, J. Inst. Metals. 62 (1938) 307–324.

[12] A. Hershey, The elasticity of an isotropic aggregate of anisotropic cubic crystals, J. of Applied Mechanics 21 (1954) 236–240.

[13] E. Kröner, Zur plastischen Verformung des Vielkristalls, Acta Metall. 9 (1961) 155–161.

[14] G. Cailletaud, Une approche micromécanique phénoménologique du comportement inélastique des métaux, Ph.D. thesis, Université Pierre et Marie Curie, Paris 6 (1987).

[15] G. Cailletaud, P. Pilvin, Utilisation de modèles polycristallins pour le calcul par éléments finis, Revue Européenne des Éléments Finis 3 (1994) 515–541.

[16] P. Pilvin, The contribution of micromechanical approaches to the modelling of inelastic behaviour, in: A. Pineau, G. Cailletaud, T. Lindley (Eds.), 4th Int. Conf. on Biaxial/multiaxial Fatigue, Saint–Germain, France, Vol. 1, ESIS, 1994, pp. 31–46.

[17] G. Martin, N. Ochoa, K. Sai, E. Hervé-Luanco, G. Cailletaud, A multiscale model for the elastoviscoplastic behavior of directionally solidified alloys: Application to FE structural computations, Int. J. Sol. Structures 51 (2014) 1175–1187.

[18] L. Méric, P. Poubanne, G. Cailletaud, Single crystal modeling for structural calculations. Part 1: Model presentation, J. of Engng. Mat. Technol. 113 (1991) 162–170.

[19] W. Ludwig, A. King, P. Reischig, M. Herbig, E. Lauridsen, S. Schmidt, H. Proudhon, S. Forest, P. Cloetens, S. R. du Roscoat, J. Buffière, T. Marrow, H. Poulsen, New opportunities for 3D materials science of polycrystalline materials at the micrometre lengthscale by combined use of X-ray diffraction and X-ray imaging, Materials Science and Engineering A 524 (2009) 69–76.

[20] D. Raabe, M. Sachtleber, Z. Zhao, F. Roters, S. Zaefferer, Micromechanical and macromechanical effects in grain scale polycrystal plasticity experimentation and simulation, Acta Metall. 49 (1981) 3433–3441.

[21] S. Forest, G. Cailletaud, D. Jeulin, F. Feyel, I. Galliet, V. Mounoury, S. Quilici, Introduction au calcul de microstructures, Mécanique et Industrie 3 (2002) 439–456.

[22] F. Roters, P. Eisenlohr, L. Hantcherli, D. Tjahjanto, T. Bieler, D. Raabe, Overview of constitutive laws, kinematics, homogenization and multiscale methods in crystal plasticity finite-element modeling: Theory, experiments, applications, Acta Mat. 58 (2010) 1152–1211.

[23] H. Moulinec, P. Suquet, A numerical method for computing the overall response of nonlinear composites with complex microstructure, Comp. Meth. Appl. Mech. Engng 157 (1998) 69–94.

[24] R. Lebensohn, N-site modeling of a 3D viscoplastic polycrystal using Fast Fourier Transform, Acta Mat. 49 (2001) 2723–2737.

[25] P. Ponte Castañeda, The effective mechanical properties of nonlinear isotropic composites, J. Mech. Phys. Sol. 39 (1991) 45–71.

[26] P. Ponte Castañeda, P. Suquet, Nonlinear composites, Advances in Appl. Mech. 34 (1998) 171–302.

[27] G. Dvorak, Y. Bahei-El-Din, A. Wafa, Implementation of the transformation field analysis for inelastic composite materials, Computational Mechanics (1994) 201–228.

[28] J.-L. Chaboche, P. Kanouté, A. Roos, On the capabilities of mean-field approaches for the description of plasticity in metal matrix composites, Int. J. of Plasticity (2005) 1409–1434.

[29] J. Eshelby, The determination of the elastic field of an ellipsoidal inclusion, and related problems, Proc. Royal Soc. London 241 (1957) 376–396.

[30] R. Hill, Continuum micro–mechanisms of elastoplastic polycrystals, J. Mech. Phys. Sol. 13 (1965) 89–101.

[31] G. Dvorak, Transformation Field Analysis of Inelastic Composite Materials, Proc. Royal Soc. London, A 437 (1992) 311–327.

[32] J.-C. Michel, P. Suquet, Nonuniform transformation field analysis: a reduced model for multiscale nonlinear problems in solid mechanics, Imperial College Press, London, 2009, pp. 156–206.

[33] B. Budianski, T. Wu, Theoretical prediction of plastic strains of polycrystals, in: Proc. 4th US Nat. Cong. Appl. Mech., 1962, pp. 1175–1185.

[34] G. Weng, Self-consistent determination of time–dependent behavior of metals, J. of Applied Mechanics 48 (1981) 41–48.

[35] A. Zaoui, Structural morphology and constitutive behaviour of microheterogeneous materials, Springer Verlag, 1997, Ch. In: Continuum Micromechanics (P. Suquet), pp. 291–347.

[36] J. Hutchinson, Bounds and self-consistent estimates for creep of polycrystalline materials, Proc. Royal Soc.

London A348 (1966) 101–127.

[37] A. Molinari, G. Canova, S. Ahzi, A self–consistent approach to the large deformation polycrystal viscoplasticity, Acta Metall. 35 (1987) 2983–2994.

[38] R. Lebensohn, C. N. Tomé, A self-consistent anisotropic approach for the simulation of plastic deformation and texture development of polycrystals: application to zirconium alloys, Acta Metall. 41 (1993) 2611–2624.

[39] R. Masson, A. Zaoui, Self-consistent estimates for the rate-dependent elastoplastic behaviour of polycrystalline materials, J. Mech. Phys. Sol. 47 (1999) 1543–1568.

[40] R. Masson, N. Bornert, M. Suquet, A. Zaoui, An affine formulation for the prediction of the effective properties of nonlinear composites and polycrystals, J. Mech. Phys. Sol. 48 (2000) 1203–1227.

[41] Z. Hashin, The inelastic inclusion problem, Int. J. of Engng Science 7 (1969) 11–36.

[42] P. Suquet, Elements of homogeneization for inelastic solid mechanics, in: E. Sanchez-Palencia, A. Zaoui (Eds.), Homogeneization Techniques for Composite Media, Springer Verlag, Lecture notes in physics, No. 272, 1985, pp. 193–278.

[43] Y. Rougier, C. Stolz, A. Zaoui, Représentation spectrale en viscoélasticité linéaire des matériaux hétérogènes, C. R. Acad. Sci. Paris, Série II 316 (1993) 1517–1522.

[44] R. Kouddane, N. Zouhal, A. Molinari, Complex loading of viscoplastic materials: micro-macro modelling, Material Science and Engineering A175 (1994) 31–36.

[45] A. Molinari, S. Ahzi, R. Kouddane, On the self-consistent modeling of elastic-plastic behavior of polycrystals, Mech. of Materials 26 (1997) 437–62.

[46] A. Paquin, H. Sabar, M. Berveiller, Integral formulation and self-consistent modelling of elastoviscoplastic behavior of heterogeneous materials, Applied Mechanics Reviews 69 (1999) 14–35.

[47] A. Paquin, S. Berbenni, V. Favier, X. Lemoine, M. Berveiller, Micromechanical modeling of the elastic-viscoplastic behavior of polycrystalline steels, Int. J. of Plasticity 17 (2001) 1267–1302.

[48] S. Berbenni, L. Capolungo, A mori–tanaka homogenization scheme for non-linear elasto-viscoplastic heterogeneous materials based on translated fields: An affine extension, Comptes Rendus Mécanique 343 (2) (2015) 95 – 106.

[49] C. Mareau, S. Berbenni, An affine formulation for the self-consistent modeling of elasto-viscoplastic heterogeneous materials based on the translated field method, Int. J. of Plasticity 64 (2015) 134–150.

[50] H. Sabar, M. Berveiller, V. Favier, S. Berbenni, A new class of micro–macro models for elastic–viscoplastic heterogeneous materials, Int. J. Sol. Structures 39 (2002) 3257–3276.

[51] Y. Liu, P. Ponte Castañeda, Homogenization estimates for the average behavior and field fluctuations in cubic and hexagonal viscoplastic polycrystals, J. Mech. Phys. Sol. 52 (2004) 1175–1211.

[52] Y. Liu, P. Ponte Castañeda, Second-order theory for the effective behavior and field fluctuations in viscoplastic polycrystals, J. Mech. Phys. Sol. 52 (2004) 467–495.

[53] I. Doghri, L. Adam, N. Bilger, Mean-field homogenization of elasto-viscoplastic composites based on a general incrementally affine linearization method, Int. J. of Plasticity 26 (2010) 219–238.

[54] I. Doghri, L. Brassart, L. Adam, J.-S. Gérard, A second-moment incremental formulation for the mean-field homogenization of elasto-plastic composites, Int. J. of Plasticity 27 (2011) 352–371.

[55] J. Simo, R. Taylor, Consistent tangent operators for rate independent elasto-plasticity, Comp. Meth. Appl. Mech. Engng 48 (1985) 101–118.

[56] K. Sai, G. Cailletaud, Multi-mechanism models for the description of ratchetting: Effect of the scale transition rule and of the coupling between hardening variables, Int. J. of Plasticity 23 (2007) 1589–1617.

[57] S. Forest, P. Pilvin, Modelling the cyclic behaviour of two–phase single crystal nickel–base superalloys, in: A. Pineau, A. Zaoui (Eds.), Micromechanics of plasticity and damage of multiphase materials, Proc. IUTAM symposium, Kluwer academic press, Sèvres, Paris, France, 1995, pp. 51–58.

[58] G. Ausias, S. Thuillier, B. Omnès, S. Wiessner, P. Pilvin, Micro-mechanical model of TPE made of polypropylene and rubber waste, Polymer 48 (2007) 3367–3376.

[59] Z-set 8.6, Non-linear material and structure analysis suite, Version 8-6, `http://www.zset-software.com/`, accessed: 2018-01-16 (2018).

[60] N. Osipov, A.-F. Gourgues-Lorenzon, B. Marini, V. Mounoury, F. Nguyen, G. Cailletaud, FE modelling of bainitic steels using crystal plasticity, Philosophical Magasine 88 (2008) 3757–3777.

[61] T. Kanit, S. Forest, I. Galliet, V. Mounoury, D. Jeulin, Determination of the size of the representative volume element for random composites: statistical and numerical approach, Int. J. Sol. Structures 40 (2003) 3647–3679.

[62] R. MacKay, R. Dreshfield, R. Maier, Anisotropy of Nickel-base Superalloy Single Crystals, Superalloys, TMS, Seven Springs, USA, 1980, pp. 385–394.

[63] P. Caron, Y. Otha, Y. Nakogawa, T. Khan, Creep Deformation Anisotropy in Single Crystal Superalloys, Superalloys, TMS, Seven Springs, USA, 1988, pp. 215–224.

[64] G. Han, J. Yu, Y. Sun, X. Sun, Z. Hu, Anisotropic stress rupture properties of the nickel-base single crystal superalloy SRR99, Materials Science and Engineering A (2010) 5383–5390.

[65] T. Hassan, S. Kyriakides, Ratcheting of cyclically hardening and softening materials. Part I: Uniaxial behavior, Int. J. of Plasticity 10 (1994) 149–184.

[66] T. Hassan, S. Kyriakides, Ratcheting of cyclically hardening and softening materials. Part II: Multiaxial behavior, Int. J. of Plasticity 10 (1994) 185–212.

[67] D. McDowell, Stress state dependence of cyclic ratcheting behavior of two rail steels, Int. J. of Plasticity 11 (1995) 397–421.

[68] J. Chaboche, A review of some plasticity and viscoplasticity constitutive theories, Int. J. of Plasticity 24 (2008) 1642–1693.

[69] D. Abdeljaoued, I. Ben Naceur, K. Sai, G. Cailletaud, A new polycrystalline plasticity model to improve ratchetting strain prediction, Mechanics Research Communication 36 (2009) 309–315.

[70] G. Cailletaud, K. Sai, A polycrystalline model for the description of ratchetting: effect of intergranular and intragranular hardening, Materials Science and Engineering A 480 (2008) 24–39.